AD A124 321 REMOTE SENSING OF THE OPTICAL AND PHYSICAL DENSITIES OF 1/1
SMOKE DUST AND WATER CLOUDS(U) SRI INTERNATIONAL MENLO
PARK CA E E UTHE DEC 82 ARO-16692.3-GS

UNCLASSIFIED DAAG29-80-C-0003 F/G 20/6 NL

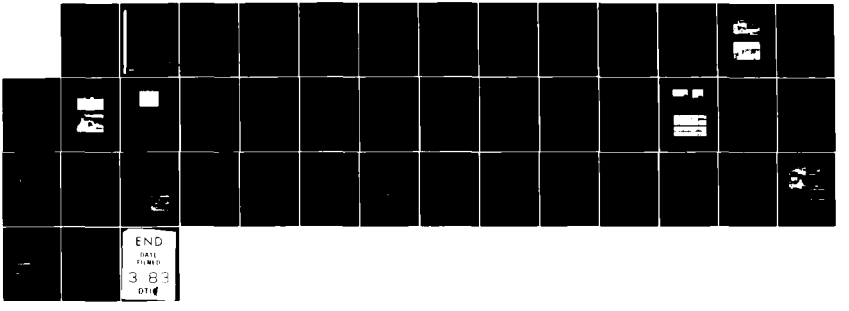

END
DATE FILMED
3 83
DTIC

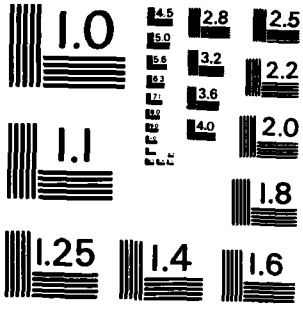

MICROCOPY RESOLUTION TEST CHART
NATIONAL BUREAU OF STANDARDS-1963-A

REMOTE SENSING OF THE OPTICAL AND PHYSICAL DENSITIES OF SMOKE, DUST, AND WATER CLOUDS

Final Report

December 1982

By: Edward E. Uthe, Director
Remote Sensing Program
Atmospheric Science Center

Prepared for:

Army Research Office
Post Office Box 12211
Research Triangle Park, North Carolina 27709

Attn: Dr. Walter Flood, Director
Geosciences Division

ARO Contract DAAG-29-80-C-0003

SRI Project 1335

SRI International
333 Ravenswood Avenue
Menlo Park, California 94025
(415) 859-6200
TWX: 910-373-2046
Telex: 334 486

THE FINDINGS IN THIS REPORT ARE NOT TO BE CONSTRUED AS AN OFFICIAL DEPARTMENT OF THE ARMY POSITION, UNLESS SO DESIGNATED BY OTHER AUTHORIZED DOCUMENTS.

Unclassified

SECURITY CLASSIFICATION OF THIS PAGE (When Data Entered)

REPORT DOCUMENTATION PAGE		READ INSTRUCTIONS BEFORE COMPLETING FORM
1. REPORT NUMBER	2. GOVT ACCESSION NO. AD-A124 321	3. RECIPIENT'S CATALOG NUMBER
4. TITLE (and Subtitle) REMOTE SENSING OF THE OPTICAL AND PHYSICAL DENSITIES OF SMOKE, DUST, AND WATER CLOUDS.		5. TYPE OF REPORT & PERIOD COVERED Final Oct 79 — Oct 82 6. PERFORMING ORG. REPORT NUMBER SRI Project 1335
7. AUTHOR(s) Edward E. Uthe, Director Remote Sensing Program Atmospheric Science Center		8. CONTRACT OR GRANT NUMBER(s) DAAG-29-80-C-0032
9. PERFORMING ORGANIZATION NAME AND ADDRESS SRI International 333 Ravenswood Avenue Menlo Park, California 94025		10. PROGRAM ELEMENT, PROJECT, TASK AREA & WORK UNIT NUMBERS
11. CONTROLLING OFFICE NAME AND ADDRESS U.S. Army Research Office Post Office Box 12211 Research Triangle Park, North Carolina 27709		12. REPORT DATE December 1982 13. NUMBER OF PAGES 36
14. MONITORING AGENCY NAME & ADDRESS(if different from Controlling Office)		15. SECURITY CLASS. (of this report) Unclassified 15a. DECLASSIFICATION/DOWNGRADING SCHEDULE NA

16. DISTRIBUTION STATEMENT (of this Report)

Approved for public release; distribution unlimited.

17. DISTRIBUTION STATEMENT (of the abstract entered in Block 20, if different from Report)

NA

18. SUPPLEMENTARY NOTES

The findings in this report are not to be construed as an official Department of the Army position, unless so designated by other authorized documents.

19. KEY WORDS (Continue on reverse side if necessary and identify by block number)

Lidar
Aerosol properties
Multiwavelength observations
Backscatter
Transmission

20. ABSTRACT (Continue on reverse side if necessary and identify by block number)

A new van-mounted four-wavelength lidar system designed for remote aerosol characterization has been constructed and tested. The most important design criteria established for the new systems was that the laser pulses should view the same path and be emitted in a minimal time period in order to reduce effects of time-variant aerosol distributions on multiple-wavelength observations.

DD FORM 1 JAN 73 1473 EDITION OF 1 NOV 65 IS OBSOLETE

Unclassified

SECURITY CLASSIFICATION OF THIS PAGE (When Data Entered)

Energy at 0.53- and 1.06-μm wavelengths is transmitted into the atmosphere using a Nd:YAG laser; 3.8 μm is transmitted using a DF laser, and 10.6 μm is transmitted using a CO_2 laser. An optical arrangement provides for transmitting the pulses along the same horizontal path, coaxial with a 12-inch-diameter Newtonian telescope. Wavelength-separation optics direct received energy to separate detectors for 0.53- and 1.06-μm energy and to a common detector for 3.8- and 10.6-μm energy. By deriving both 0.53- and 1.06-μm laser emissions from a single flash lamp excitation, and by recording the four backscatter signatures within a single transient digitizer 2048-word record, the four signatures can be collected within a 160-μs interval. Each four-wavelength lidar record is transferred to an LSI 11/2 microcomputer and written on nine-track magnetic tape, together with date and time information.

SRI conducted a field test of the four-wavelength lidar to evaluate system performance in an environment similar to that of previous lidar operations at Army range facilities. The lidar van was located about 600 m from an 8-ft square passive reflector. Both dust and smoke aerosols were generated near the midpoint of the lidar-to-target path. The lidar successfully recorded the time history of aerosol range-resolved backscatter at each of the four wavelengths. Target returns were used to evaluate time records of transmission at each of the four wavelengths. Results indicated that the lidar system is nearly ready for participation in Army field tests to further explore its use in remote aerosol characterization.

CONTENTS

ILLUSTRATIONS

I STATEMENT OF THE PROBLEM

A major concern to developers of Army electrooptical systems is system performance in the presence of battlefield obscurants such as smoke, dust, and naturally occurring haze and clouds. To evaluate obscurant effects, a series of environmental tests are being conducted to provide data on aerosol properties along paths viewed by optical instruments used to measure transmission, scattering, and path radiance for wavelength regions used by electrooptical systems.

SRI International (SRI) has been investigating the use of laser radar (lidar) to measure optical and physical properties of obscurants over extended areas--especially in the vertical--with spatial and temporal resolution not possible with in-situ sensors. The first experiments used single-wavelength lidar systems to measure variability of aerosol concentration distributions along horizontal optical paths. Analysis of backscatter signatures in terms of absolute aerosol optical and physical densities was only partially successful. Use of a constant-reflectivity passive target at the end of the lidar-observed path provided the means to derive time-dependent transmissions over the lidar-to-target path. However, the goal of the lidar program is to develop a method capable of making single-ended measurements of optical or physical density so that vertical and slant paths can be evaluated.

Absolute optical and physical-density analysis of backscatter signatures was limited on previous studies because accurate corrections for attenuation and multiple-scattering could not be determined. Attenuation correction was applied by using a solution of the single-scattering lidar equation that required assumptions on the backscatter-to-extinction relationship and on a boundary value of extinction along the observed path. Results from these tests indicated that additional information on the nature of the scattering medium was needed in order to derive useful estimates of optical and physical densities from single-ended lidar measurements. In addition, information on the importance of multiple scattering would be required to assess the usefulness of the single-scattering analysis approach and to formulate analysis methods that consider higher orders of scattering.

Upon sponsorship of the U.S. Army Research Office and U.S. Army Atmospheric Sciences Laboratory, SRI assembled a 0.7- and 10.6-μm dual-wavelength lidar system and used the lidar to observe dust and smoke aerosols during the DIRT I and Smoke Week II field programs (Appendix A). Results from these tests showed that the wavelength dependence of backscatter and attenuation provided information on particle size, and therefore that smoke particles could be distinguished from larger-sized dust particles.

For dense smoke clouds, the longer wavelength was less affected by attenuation and multiple-scattering; a higher correlation was therefore obtained between lidar-measured backscatter and extinction and aerosol concentration terms. However, at both wavelengths, relatively large data-point scatter and nonlinear relationships occurred in plots of path-integrated backscatter against optical depth (as derived from target returns). Theoretical considerations indicated that the scatter could be a result of changing particle sizes, and that observations in the 3.0- to 4.0-μm wavelength region might be less sensitive to particle-size variability. Because the extinction-to-mass-concentration ratio may be less sensitive to changes of particle size in this wavelength region, estimates of physical density from lidar backscatter signatures may be more valid.

Two other studies were recently performed at SRI to provide an evaluation of multiple-wavelength lidar techniques for characterizing the scattering medium. One study (Appendix B) used a 14-wavelength transmissometer to make extinction measurements of aerosols generated with particles of different composition, size, and shape distributions. The collected data indicated that mean particle size smaller than 1-μm diameter could reasonably be estimated from measurements made using a single-laser lidar system operating at 0.53- and 10.6-μm wavelengths. For larger mean particle sizes, the extinction ratio is near one and longer-wavelength systems are required. The data indicated that a two-laser lidar operating at 10.6 and 0.53 μm could provide estimates of mean particle size to diameters of at least 6 μm.

The second study (Appendix C) applied the results of the multiple-wavelength transmissometer study (discussed above) and two-wavelength (0.53 and 1.06 μm) airborne lidar measurements to infer the mean particle size of forest fire smokes from a remote distance. Although in-situ verification data were not collected, the lidar particle-size results agreed well with previous in-plume sampling of combustion aerosols.

The objective of the program reported upon herein was to develop a 3- to 4-μm wavelength lidar system to be used in conjunction with the two-wavelength system used on earlier studies, and to evaluate the capabilities of the three-wavelength system for making quantitative measurements of aerosol optical and physical densities. However, subsequent analysis of data collected during Smoke Week II (see Appendix A) showed that the lidar observations of Army-generated smoke and dust clouds at different wavelengths must be made along the same path--rather than separated paths as was necessary with the 0.7/1.06-μm wavelength system.

It was therefore determined that a new lidar system using coaxial multiwavelength laser emissions would greatly facilitate the development of remote aerosol characterization techniques. This report describes the four-wavelength lidar system that was designed and constructed and presents some preliminary results obtained through observation of smoke and dust aerosols.

II FOUR-WAVELENGTH LIDAR SYSTEM

The most important design criteria established for the multiwavelength lidar was that the laser pulses should view the same path and be emitted in a minimal time period in order to reduce effects of time-variant aerosol distributions on the multiwavelength observations. Wavelengths of 0.53, 1.06, 3.8, and 10.6 μm were chosen because they are important to current Department of Defense (DoD) electrooptical systems, and because a wide wavelength range is needed to analyze scattering data in terms of aerosol properties. Energy at 0.53 and 1.06 μm is obtained from a Nd:YAG laser, 3.8 μm from a deuterium fluoride (DF) laser, and 10.6 μm from a CO_2 laser. These lasers were available from previous studies or were purchased on this project. The design utilized other lidar components already available at SRI. SRI purchased a 7-m van so that the lidar could be constructed as a mobile unit, which could easily be transported to various field sites.

Figure 1 presents a block diagram of the lidar system; Figure 2 presents external and internal views of the lidar van. The three lasers and a 12-inch Newtonian telescope (coated for 10.6-μm wavelength) were mounted on a specially constructed optical table. Optics needed to direct the laser pulses coaxial with the telescope are contained in an enclosure constructed along one edge of the optical table. The current design accommodates only horizontal or vertical measurements, but can be modified to include scanning optics for slant-path measurements. Each laser face has been fitted with a beam-splitter and pyroelectric detector to provide zero time triggers to initiate data collection by the digital data system, and to provide a signal proportional to laser emitted peak power. Because the data system uses only a single transient digitizer (Biomation 8100), the Nd:YAG laser is pulsed twice to obtain both 0.53- and 1.06-μm lidar signatures. The laser is pulsed twice with a single flashlamp excitation (double pulse mode) so that both laser pulses can be transmitted within a 50-μs interval. The 3.8-μm laser is pulsed about 50 μs following the final Nd:YAG pulse, and the 10.6-μm laser is pulsed about 50 μs later. Thus, all four laser pulses are emitted within an approximately 160-μs interval to minimize effects of time-variant aerosol distributions along the observed path.

Backscatter energy from the four-wavelength laser emissions is collected by a 12-inch Newtonian telescope and optically focused on a three-detector receiver package mounted on the telescope housing. A dichroic filter directs the 3.8- and 10.6-μm wavelength energy to a HgCdTe liquid-nitorgen-cooled detector, while passing the 0.53- and 1.06-μm wavelength energy to a second dichroic filter. The second filter directs 0.53-μm energy on the surface of a silicon avalanche detector and the 1.06-μm energy on the surface of a second silicon avalanche detector. Output of

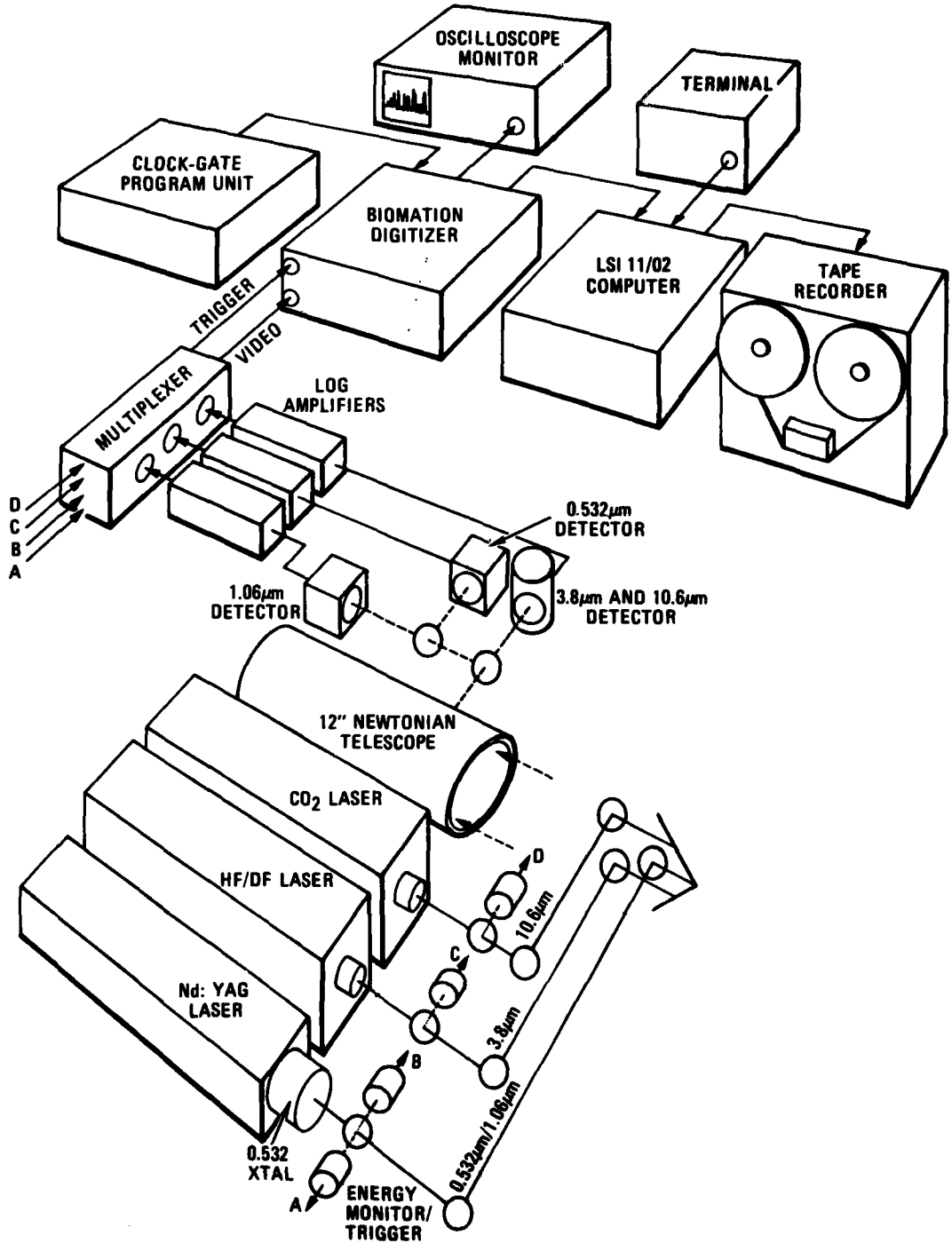

FIGURE 1 BLOCK DIAGRAM OF THE FOUR-WAVELENGTH LIDAR SYSTEM FOR REMOTE AEROSOL MEASUREMENT

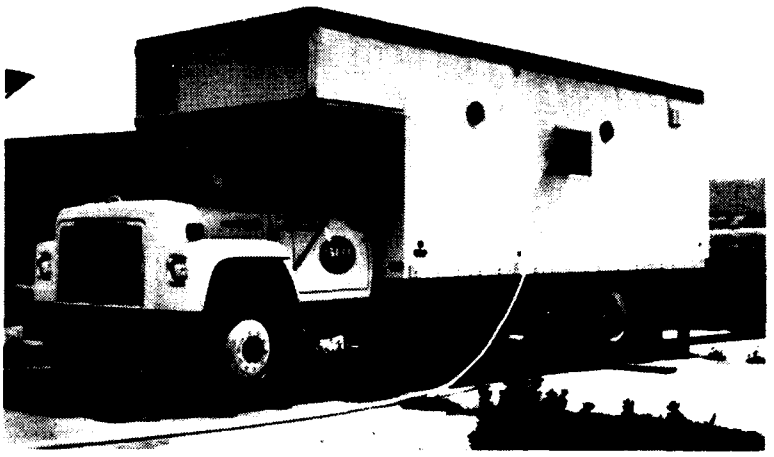

(a) EXTERNAL VIEW SHOWING LASER PORT FOR HORIZONTAL MEASUREMENTS

(b) INTERNAL VIEW SHOWING LASER/OPTICS TABLE AND DATA RECORDING SYSTEM

FIGURE 2 FOUR-WAVELENGTH LIDAR SYSTEM IN 6-METER-LONG VAN

detectors is input to video logarithmic amplifiers each of which has about four orders of magnitude response. The time-dependent signals are then digitized by a Biomation 8100 transient recorder.

A multiplexer combines the analog backscatter signatures for input to the single transient digitizer. Each waveform consists of the output from an energy monitor and lidar detector. The Biomation 8100 provides 2048 8-bit words with sample intervals of 10, 20, or 50 μs (150-m range per μs). A clock-gate unit was designed and constructed to interrupt the Biomation's digitization process so that backscatter signatures from all four wavelength pulses can be stored in a single 2048-word record. The digitization is controlled by a timing sequence that is initiated by laser fire pulses, so that digitization is in progress when the energy monitor pulse from each laser is generated. Therefore, the energy monitor pulse and backscatter signature for each of the four wavelengths are recorded within about 500 Biomation words of the complete 2048-word record. At the conclusion of the digitization for the fourth laser firing, the full Biomation record is transferred to an LSI 11/02 microcomputer using direct memory access (DMA). The computer formats the lidar data and date and time information and writes the record on a nine-track 1600 bit/inch magnetic tape recorder. Recorded tapes can be read back by the computer; values may be printed or graphed on a hardcopy terminal. Data evaluations using the data collection system thus facilitate field evaluation of recorded records.

III SYSTEM TEST AND RESULTS

SRI conducted a test of the four-wavelength lidar to evaluate system performance in an environment similar to those experienced during previous lidar operations at Army range facilities (Appendix A). The lidar van was located about 600 m from an 8-ft square passive reflector constructed on the field site, located at Stanford University (Figure 3). Both dust and smoke aerosols were generated near the midpoint of the lidar-to-target path. Four wavelength lidar observations of the generated aerosol plumes were recorded on magnetic tape. Figure 4 presents an example of a Biomation record as displayed on the oscilloscope monitor (shown in Figure 1) during a dust test. (The energy monitor pulses were not yet incorporated into the Biomation record when these data were collected.) The larger ratio of dust-to-clear-air backscatter for longer wavelengths is expected, because dust (large-particle) scattering is nearly wavelength independent, but clear-air scattering is proportional to the inverse fourth power of wavelength (assuming Rayleigh scattering).

Quantitative evaluation of lidar backscatter signatures requires information relating observed signal (detector voltage or digitizer counts) to intensity of light incident on the detector. A preliminary receiver calibration for each of the four wavelengths was derived by placing neutral density optical filters in front of the detectors and relating reduction of lidar-observed target signals (Figure 4) to known attenuation of the optical filters. Results of the detector calibration for each of the four wavelengths are shown in Figure 5.

Figure 6 presents an example of a computer display generated from backscatter signatures recorded on magnetic tape during red smoke observation. The dashed lines present clear-air backscatter signatures recorded before the start of the smoke test. After smoke detection, the target returns diminish because of two-way attenuation of the laser pulses as they penetrate the smoke plume. The shapes of the target returns reflect the laser pulse characteristics. The target returns in Figure 6 show that highest resolution (i.e. shortest pulse length) is provided by the 1.06-μm laser. The DF laser (3.8 μm) has the longest pulse length and therefore the lowest range resolution.

Range-resolved backscatter increases between solid and dashed lines in Figure 6 are a result of increased scattering by smoke particles distributed along the lidar-observed path. The effect of pulse length on the observed smoke distribution is clearly evident and must be considered in any multiple-wavelength analysis of plume backscatter data.

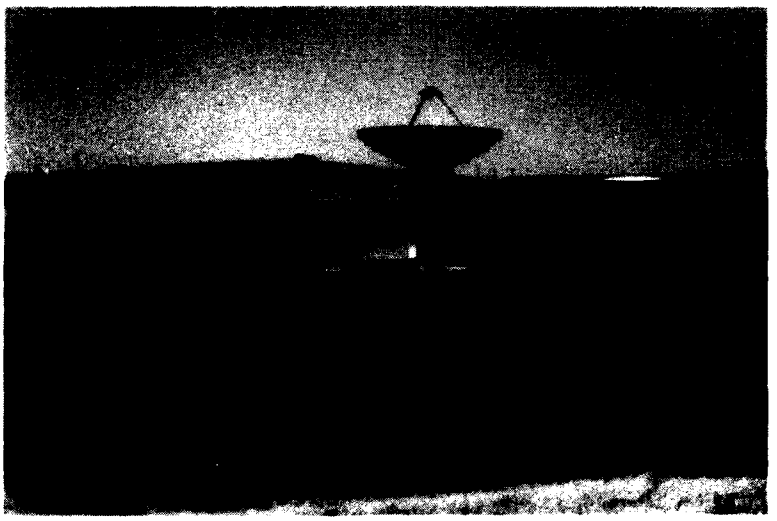

(a) LIDAR VAN AT TEST SITE

(b) 8-ft SQUARE PASSIVE REFLECTOR (600-m from lidar)

FIGURE 3 SYSTEM TEST ENVIRONMENT AT STANFORD UNIVERSITY

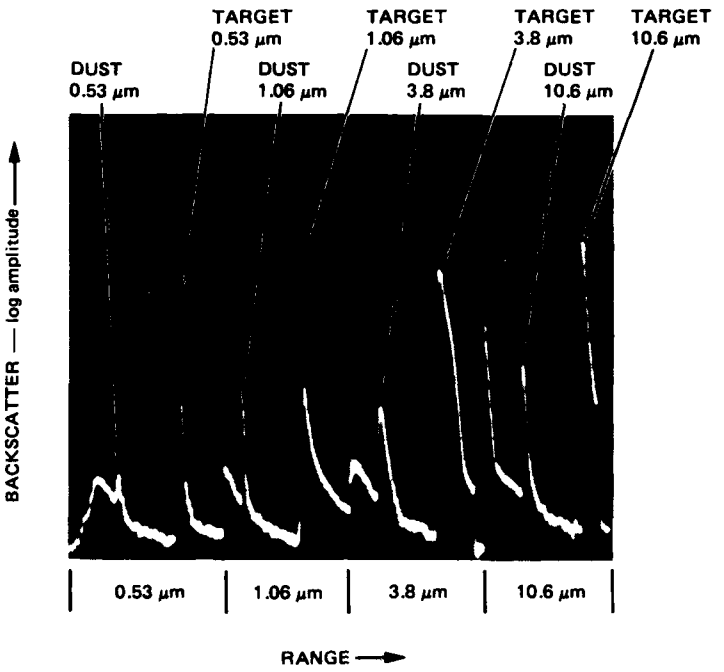

FIGURE 4 FOUR-WAVELENGTH LIDAR BACKSCATTER SIGNATURE FOR DUST GENERATED ALONG 600m PATH BETWEEN LIDAR AND TARGET

Stanford Field Site, 7 July 1982.

The target returns provide a means to evaluate obscurant transmission along the lidar-to-target path quantitatively. Transmission values determined from a single firing of each laser are given in Figure 6. Figure 7 presents a time history of transmission derived from data collected during a red-smoke test. These data indicate the optical properties of smoke are nearly equal at 0.53 and 1.06 μm, with substantially less attenuation at 3.8 μm and almost no attenuation at 10.6 μm. However, these results are based on a preliminary calibration of the four-wavelength lidar; further calibration is needed to confirm the results. More extensive calibrations using optical filters of known attenuation are planned. Transmission values evaluated from target returns can be used to develop and validate transmission values derived from the range-resolved backscatter data, so that measurements can be made along vertical and slant paths.

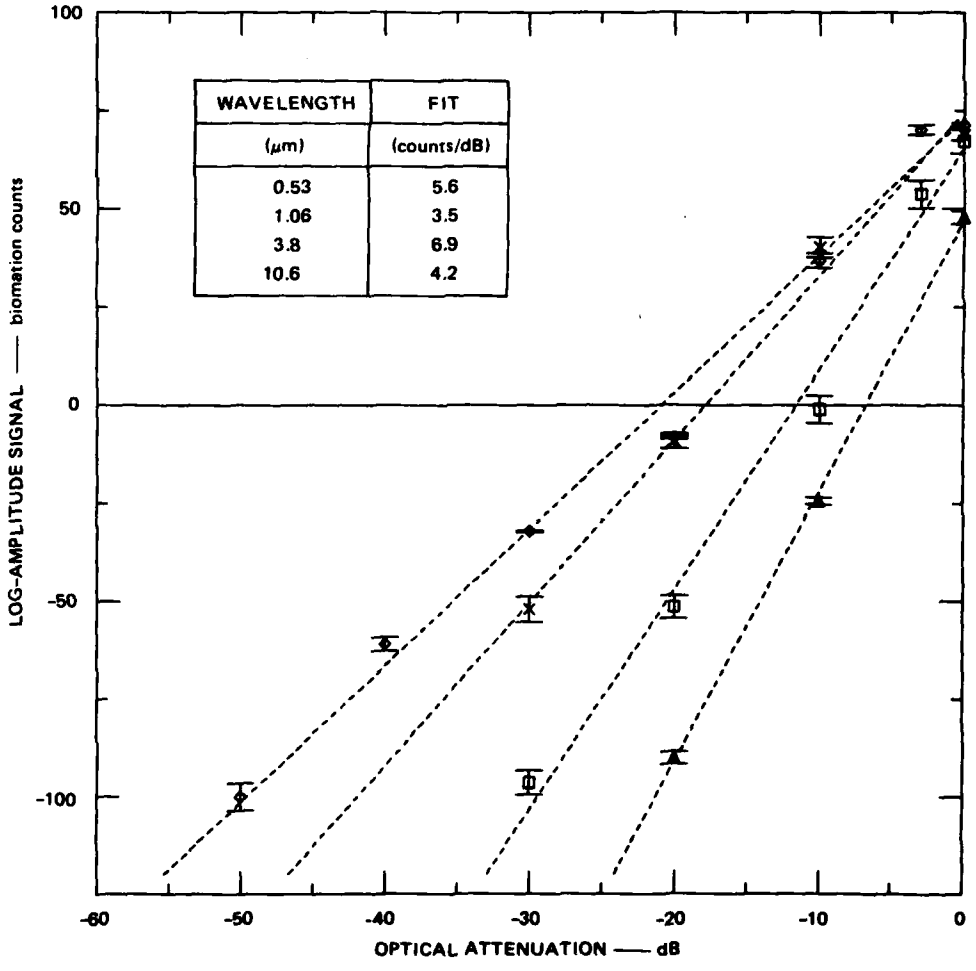

FIGURE 5 DETECTOR CALIBRATION RESULTS FOR SRI FOUR-WAVELENGTH LIDAR

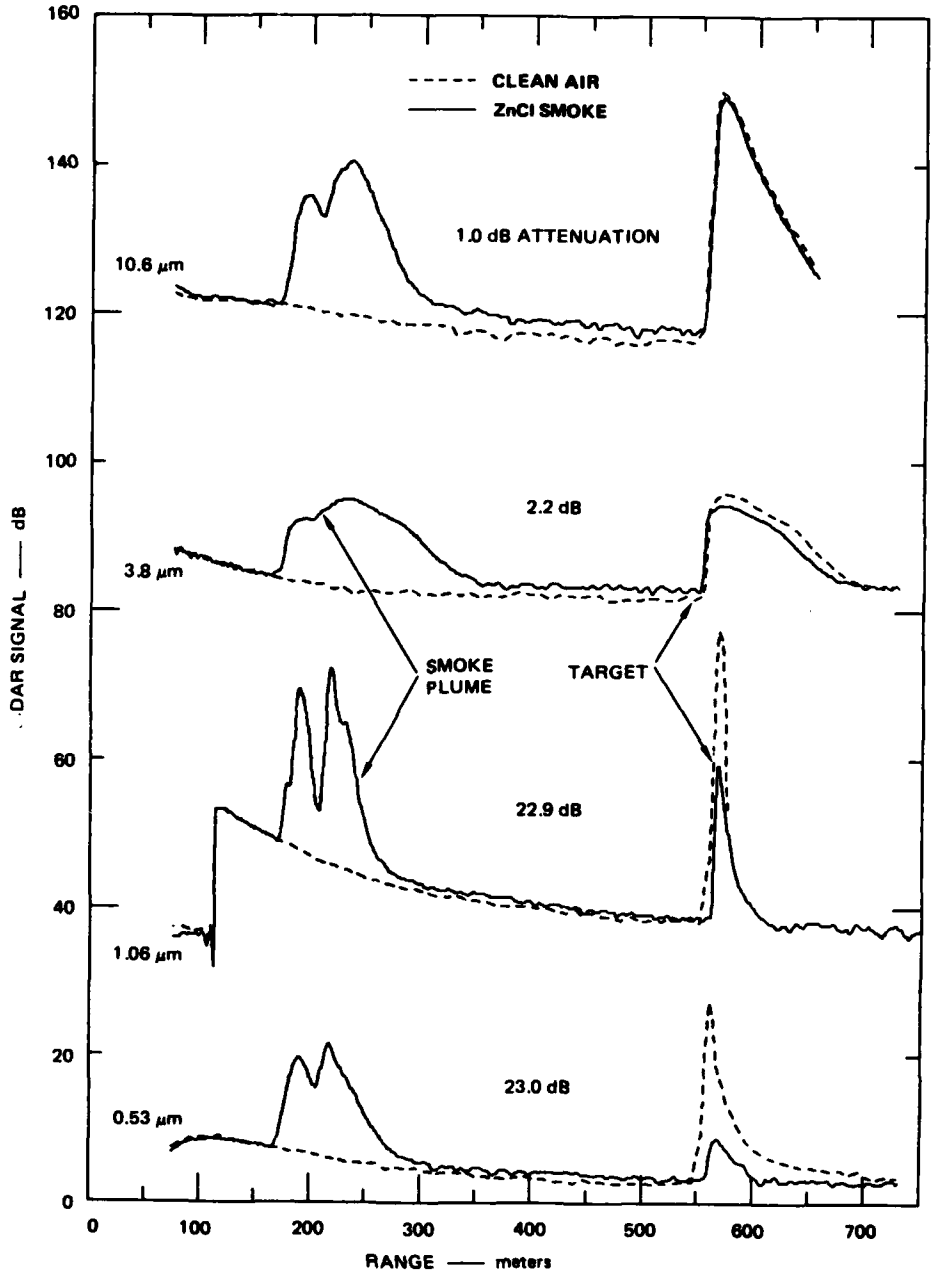

FIGURE 6 FOUR-WAVELENGTH LIDAR BACKSCATTER SIGNATURES AND SMOKE ATTENUATION DERIVED FROM TARGET RETURNS USING PRELIMINARY CALIBRATIONS

Stanford Field Site, 8 July 1982

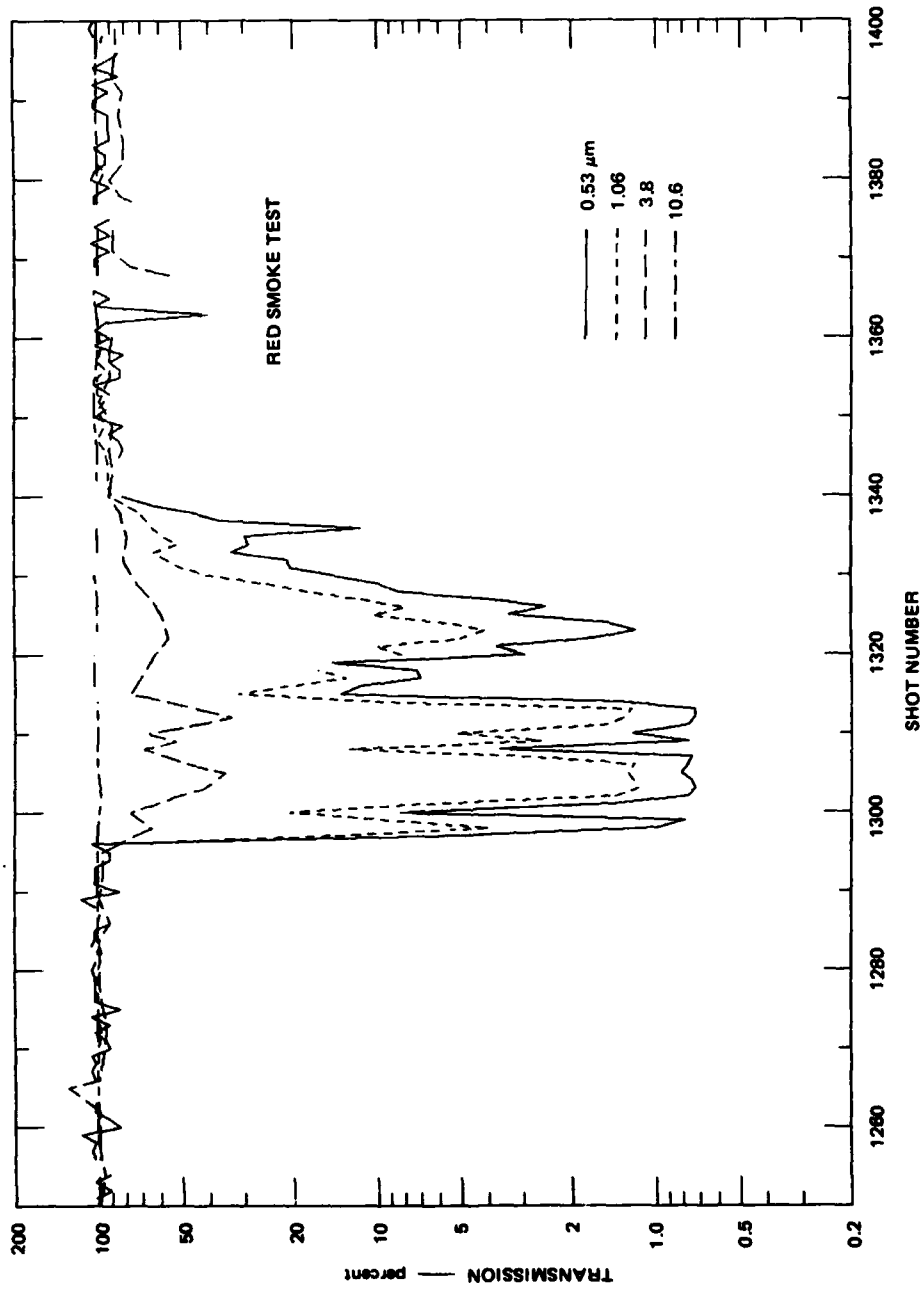

FIGURE 7 LIDAR TEST TRANSMISSION HISTORY

IV CONCLUSIONS

A four-wavelength lidar system has been constructed for use in developing and validating lidar techniques for remote evaluation of obscurent properties. The new system provides means for making nearly simultaneous multiwavelength observations over nearly identical atmospheric paths--a requirement established on previous lidar studies. The system uses 0.53, 1.06, 3.8, and 10.6 μm laser wavelengths, which are the wavelengths most used by DoD electrooptical system designers. The lidar should therefore be useful in evaluating atmospheric effects during field testing of various electrooptical systems, and the wide wavelength range should provide the means to characterize aerosol properties (such as particle size distribution) as an aid to determining attenuation and multiple scattering terms. These optical effects must be accounted for before useful aerosol densities can be evaluated from lidar backscatter measurements.

The four-wavelength lidar was tested by observing smoke and dust aerosols generated at a field site at Stanford University. Although only preliminary calibrations were available, reasonable transmission results were obtained, indicating that the four-wavelength system is nearly ready for participation in more extensive tests. SRI plans to conduct more extensive calibration experiments and participate in future range testing of environmental effects on electrooptical systems such as the DIRT, Smoke Week, and SNOW series.

V LIST OF PUBLICATIONS

The items listed below were published or presented during the course of this project:

- Uthe, E.E., 1981: "Lidar Evaluation of Smoke and Dust Clouds," Applied Optics, Vol. 20, pp. 1503-1510.*
- Uthe, E.E., 1982: "ALPHA-1/ALARM Airborne Lidar Systems and Measurements," Proceedings of the Workshop on Optical and Laser Remote Sensing, Monterey, California, sponsored by the Army Research Office (February).
- Uthe, E E., 1981: "Lidar Evaluation of Smoke and Dust Clouds," Proceedings of the Smoke/Obscurants Symposium V, Harry Diamond Laboratories, Adelphi, Maryland, sponsored by the Office of the Project Manager, Smoke and Obscurants (April).

*Appendix A of this report

VI PARTICIPATING SCIENTIFIC PERSONNEL

SRI staff members who participated in the research effort are listed below:

- Edward E. Uthe, Director, Remote Sensing Program
- Warren B. Johnson, Director, Atmospheric Science Center
- Norm B. Nielsen, Field Engineering Representative
- Jan van der Laan, Senior Research Engineer
- Stephen A. DeLateur, Research Engineer
- John M. Livingston, Research Meteorologist.

None of the project staff earned advanced degrees during the course of the project.

Appendix A

LIDAR EVALUATION OF SMOKE AND DUST CLOUDS*

*Applied Optics, Vol. 20, pp. 1503-1510 (1981).

Lidar evaluation of smoke and dust clouds

Edward E. Uthe

Lidar provides the means to evaluate quantitatively the spatial and temporal variability of smoke and dust clouds as they are transported downwind from particulate sources. Quantitative evaluation of cloud optical and physical densities from cloud backscatter is complicated by effects from particle size, shape, and composition and by attenuation and multiple scattering for dense clouds. Examples are presented that review use of the lidar technique to provide useful evaluations of smoke and dust clouds.

I. Introduction

Laser radiation is effectively scattered by particulate material suspended in the atmosphere and can be transmitted over long atmospheric distances as short-duration high-energy pulses directed along well-collimated beams. Using these properties, researchers have developed laser radar systems to observe clear-air atmospheric structure over extended areas with high resolution in space and time.[1,2] For atmospheric conditions of relatively high visibility, the effects of aerosol attenuation and multiple scattering are slight, and range-resolved backscatter observed by the lidar technique has been equated to the distribution of particulate concentrations along the propagation path. For atmospheres containing higher particulate concentrations, however, attenuation and multiple scattering may complicate the relation of observed backscatter to particle concentration distributions. Moreover, variations of particle size, shape, and composition along the observed path introduce uncertainties in the interpretation of the lidar signature. Nevertheless, lidar is the most effective method available to derive information on distant particle concentrations. This paper presents data examples, collected during several field programs, that demonstrate the usefulness of lidar for remote evaluation of smoke and dust clouds.

The author is with SRI International, Atmospheric Science Center, Menlo Park, California 94025.

Received 13 September 1980.
0003-6935/81/091503-08$00.50/0.

II. Lidar Evaluation of Cloud Distributions

The atmosphere is typically a highly variable medium, causing complex transport and diffusion of particulate clouds downwind of their sources. Because conventional measurement methods cannot adequately determine the spatial and temporal variability of particle concentration distributions over extended atmospheric regions, establishing limiting effects of particulate clouds on various electrooptical systems is difficult. Lidar provides a means to derive quantitative information on particulate cloud distributions and optical properties over remote distances using instrumentation located at a single convenient location. For example, Fig. 1 presents a lidar-derived vertical cross section through a smoke plume that provides information on the location and dimension of the plume and on the distribution of particulate concentrations within it. Representative cross sections made at about half-minute intervals provide data on both instantaneous and time-averaged cloud geometry. A second example, Fig. 2, illustrates the use of lidar during a weapon firing exercise. Information is provided on both the smoke cloud generated at the weapon site and the dust cloud generated at the impact area.

The U.S. Army recently conducted a series of smoke and dust tests using lidar and transmissometer instrumentation to derive time records of optical properties along a near surface horizontal path that intersected generated smoke and dust clouds, as illustrated in Fig. 3. A passive reflector terminated the lidar path so that transmission over the path could be evaluated from lidar-observed target returns. During Smoke Week II (Eglin Air Force Base, 6–16 Nov. 1978), a 10.6-μm wavelength lidar was operated by the U.S. Army Atmospheric Science Laboratory (ASL) and a 0.7-μm wavelength lidar (Mark IX) was operated by SRI in the manner shown in Fig. 3. Backscatter data from both lidars were recorded and processed by the data system of the Mark IX lidar to facilitate two-wavelength

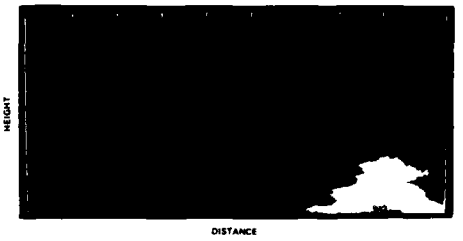

Fig. 1. Example of computer-generated vertical plume density profiles. Lidar is located at lower left corner. The height and distance scale is 75 m/div. Plume vertical concentrations (relative to clear air with a scale of 10 dB/div) are plotted at the lower left, and the horizontal position associated with each profile is plotted in the upper right.

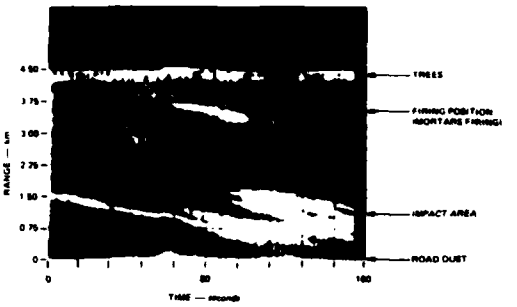

Fig. 2. Lidar-derived distance/time cross section of aerosol structure resulting from mortar firing and impact.

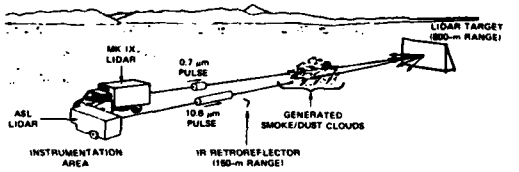

Fig. 3. Experiment configuration of two-wavelength lidar observations during Smoke Week II.

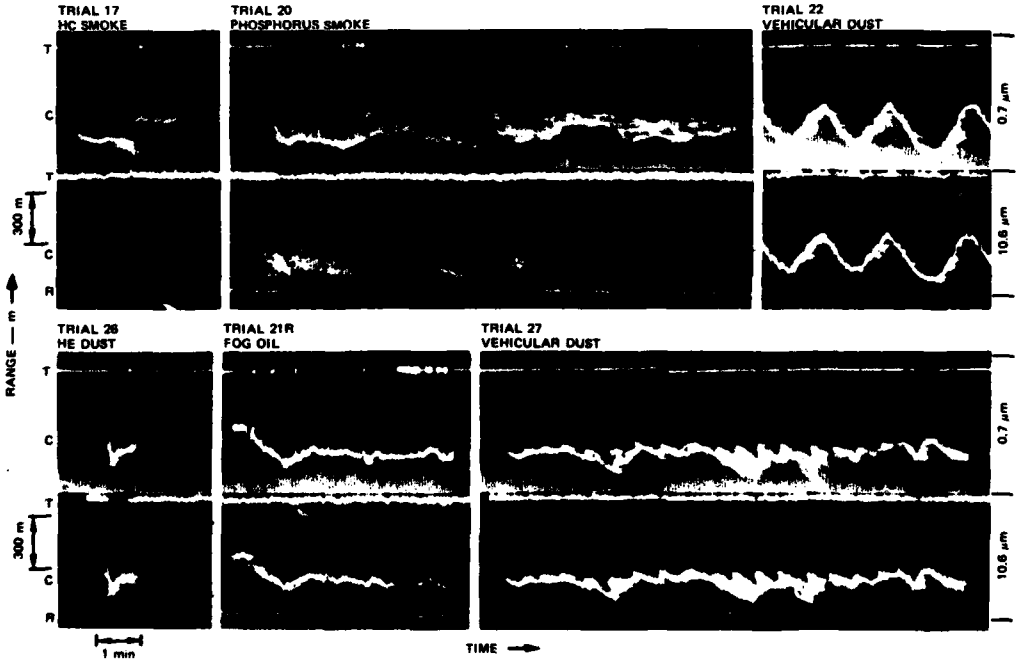

Fig. 4. Range/time intensity-modulated displays depicting lidar-observed structure along instrumented path intersected by aerosol clouds generated during Smoke Week II. Upper record is from SRI 0.7-μm wavelength lidar and lower record is from ASL 10.6-μm wavelength lidar. Target, cloud, and retroreflector (IR only) are indicated by the letters *T*, *C*, and *R*, respectively.

analysis of collected records. Figure 4 presents intensity modulated range/time cross sections of cloud distributions observed by the two-lidar system during several Smoke Week II trials. These records provide information on the space and time variability of aerosol density along the observed path. The data also indicate that the wavelength dependency of cloud optical properties depends on aerosol type.

III. Lidar Evaluation of Cloud Optical Density

A. Attenuation Estimates Derived from Target Returns

Transmission of laser energy over a lidar-to-target path can be estimated from the magnitude of lidar-observed target returns. During the Smoke Week II tests, visible and infrared lidars viewed paths nearly coincident with paths viewed by conventional two-ended transmissometers operated by the Dugway Proving Ground. Therefore, lidar-derived transmissions can be evaluated against transmissometer records in the manner shown in Fig. 5 for three Smoke Week II trials (HE dust is generated from high-explosive events conducted near the earth's surface). The lidar and transmissometer values agreed relatively well in the sixteen trials analyzed except in most of those with phosphorus clouds; the density of those clouds varies greatly with their height above ground, and the lidar and transmissometer paths were separated by ~2 m in elevation. Nevertheless, the agreement obtained for most observations validated the lidar/target method of measuring cloud attenuation. Although this method requires a passive reflector at the end of the lidar path, observations over a variety of horizontal paths can be made by use of multiple reflectors, and observations for slant paths can be made if elevated targets are installed.

B. Attenuation Estimates Derived from Cloud Backscatter

The major objective of the Smoke Week II lidar study was to determine the feasibility of making attenuation measurements for dense aerosol clouds by analyzing lidar backscatter from the cloud. By this method, measurements could be made along a variety of slant paths through the cloud at different downwind distances from the emission source.

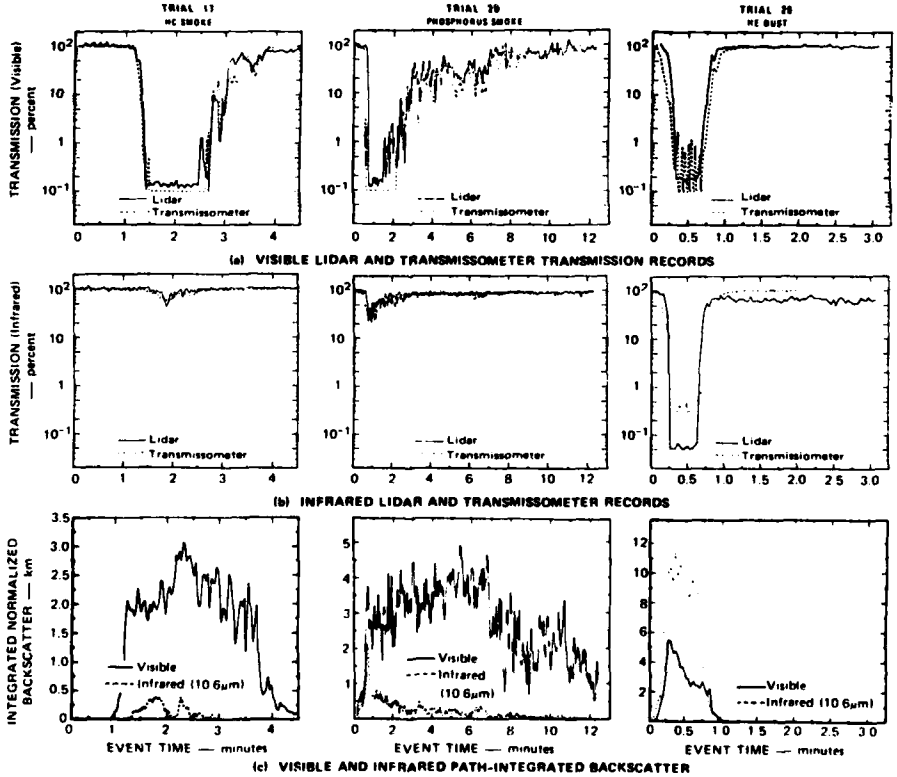

Fig. 5. Comparison of transmissions derived from lidar target returns and transmissometer records for (a) visible, (b) infrared systems, and (c) path-integrated backscatter for three Smoke Week II trials.

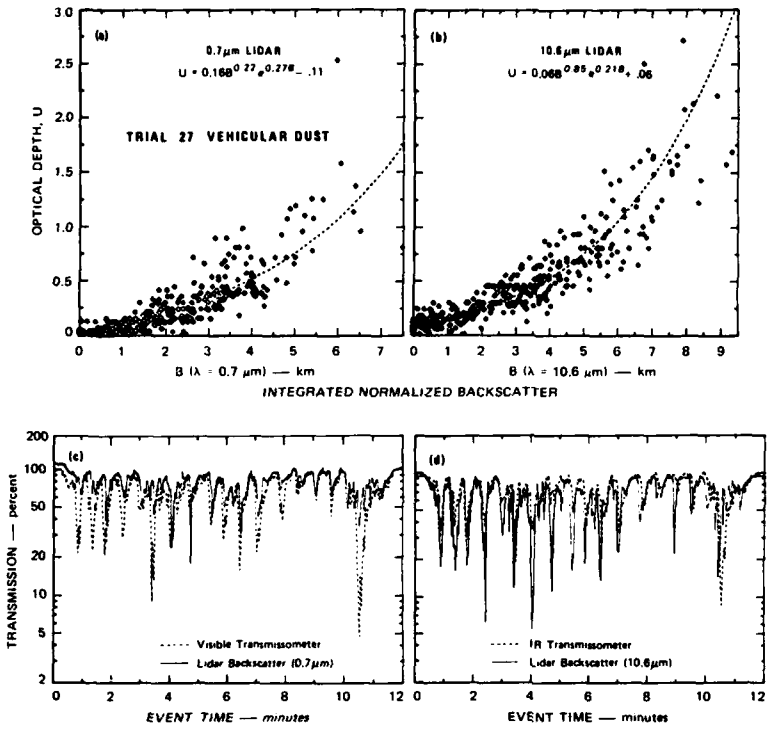

Fig. 6. Lidar-derived relationship between cloud optical depth and path-integrated backscatter (a) and (b) and comparison of lidar backscatter-derived transmissions with transmissometer records (c) and (d).

For each of the sixteen smoke or dust events analyzed, the path-integrated backscatter from the cloud normalized to clear-air backscatter was evaluated as a function of event time. Figure 5(c) presents the visible and infrared path-integrated backscatter for trials 17, 20, and 26. The results show that the wavelength dependence of attenuation and backscatter is a good indicator of aerosol type. Plots of optical depth ($U = -\ln T$, T = transmission) evaluated from the target returns and path-integrated backscatter evaluated from the cloud returns typically showed that these parameters are related in a nonlinear manner as shown, for example, in Figs. 6(a) and (b) for vehicular dust (trial 27). The greatest data scatter between these parameters usually occurred for smoke particles. At larger values of optical depth, the integrated backscatter normally becomes independent of optical depth primarily because backscatter from the far side of the cloud is not observed, being attenuated by particles in the near side of the cloud. For several phosphorus events, integrated backscatter increased with increasing optical depth but decreased with further increases in optical depth. Therefore, both data scatter and nonuniqueness of the optical depth-to-backscatter relationship must be addressed as limitations to applying the lidar technique for single-ended measurements of cloud attenuation.

The nonlinear expressions in Figs. 6(a) and (b) and path-integrated backscatter values were used to derive the time-dependent transmission record that is compared with the Dugway transmissometer record in Figs. 6(c) and (d). The lidar backscatter data reproduce the general features of the transmissometer trace. These results indicate that useful information on cloud attenuation can be derived from cloud backscatter data, providing that the optical depth-to-integrated backscatter expression remains valid for a wide range of dust aerosols. In practice, a vertically scanning lidar could observe a passive reflector terminating the near-surface path to derive the calibration data necessary to interpret slant-path transmissions.

Another example of deriving cloud attenuation data from cloud backscatter data is shown in Fig. 7 for a phosphorus event. The optical depth and integrated backscatter data derived at the visible wavelength indicated that valid transmissions could be evaluated from backscatter data only for optical depths of <1.0. However, as shown in Fig. 7(a), infrared path-integrated backscatter is a relatively good indicator of visible optical depths for clouds extending to optical depths of 6.0. Using the expressions shown in Fig. 7(a) and the infrared backscatter data, a time-dependent trace of visible transmission was derived and compared with visible transmissions evaluated from target returns [Fig. 7(b)] and with visible transmissometer data [Fig. 7(c)]. The discrepancy with the transmissometer data was expected because the visible lidar and transmissometer paths were separated by 2 m in elevation, and phos-

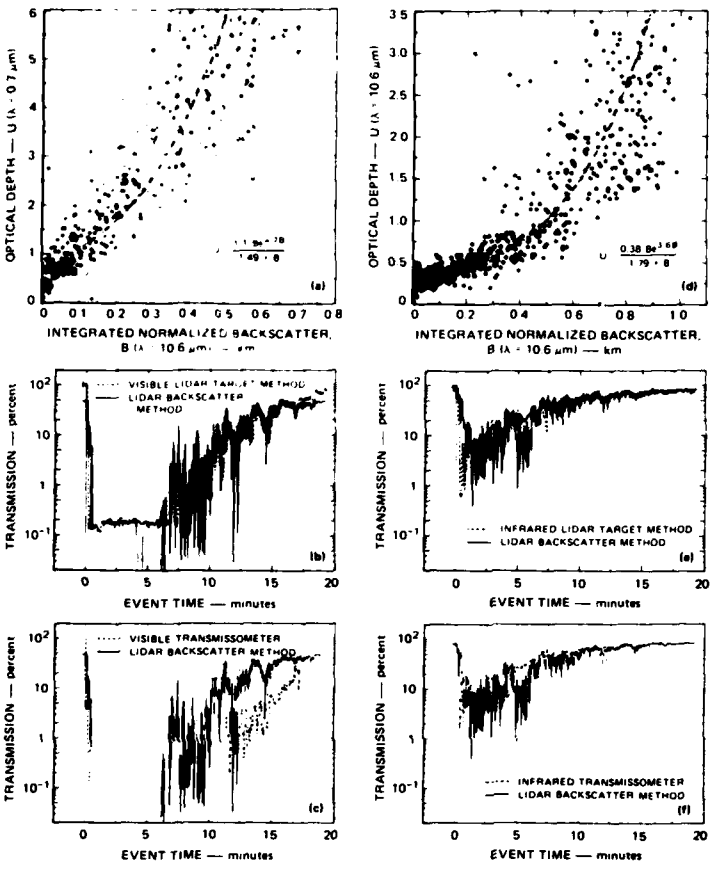

Fig. 7. Derivations of optical depth-integrated backscatter expressions and comparisons of transmissions derived from lidar target, lidar backscatter, and transmissometer methods. Expressions derived are (a) between visible optical depth and infrared integrated backscatter and (d) between infrared optical depth and infrared integrated backscatter. Comparisons of backscatter-derived transmissions and those derived from lidar target and transmissometer records are shown in (b), (c), (e), and (f).

phorus cloud density varied greatly with its height above ground.

Figures 7(d), (e), and (f) show the derivation of infrared transmissions from infrared backscatter data and comparisons with results obtained from the lidar target method and with the transmissometer record. These data indicate that the 10.6-μm wavelength can provide useful estimates of both visible and infrared transmission through dense smoke clouds.

IV. Lidar Evaluation of Cloud Type

The results of the Smoke Week II study indicate that wavelength dependence of cloud attenuation and backscatter provide information on cloud type. Dust clouds could easily be distinguished from smoke clouds as large wavelength dependence indicates small particle sizes of smoke aerosols, whereas small wavelength dependence indicates larger particle sizes of dust aerosols. Other examples of the use of lidar to evaluate cloud type are presented below.

Figure 8 presents data derived from backscatter signatures recorded while the lidar was observing black

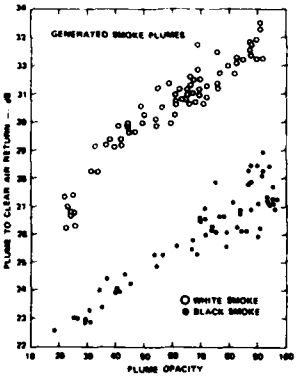

Fig. 8. Plume returns plotted against opacities derived from near- and far-side clear-air returns.

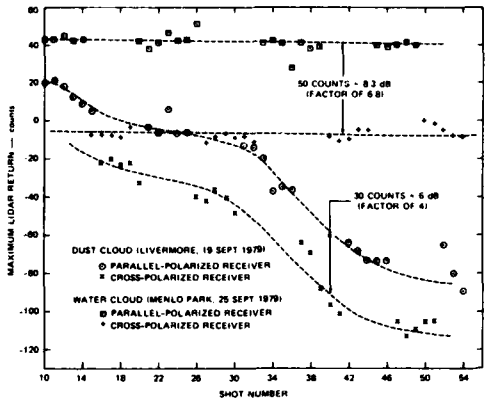

Fig. 9. Parallel- and cross-polarization backscatter observations of dust and water clouds made with the Mark IX lidar.

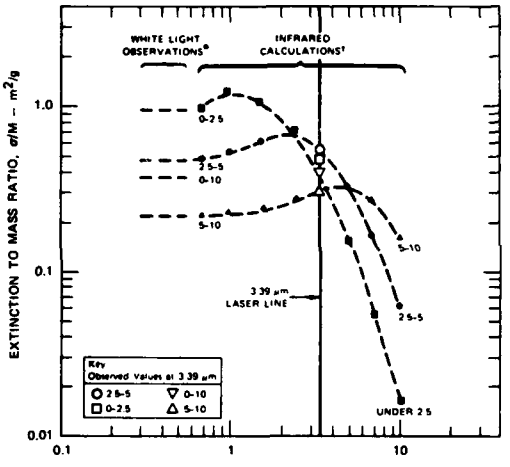

*Values measured by Uthe and Lapple for fly ash aerosols with 0-2.5, 2.5-5, 5-10, and 0-10 μm diameter size fractions.

†Based on log normal size distributions fitted to measured fly ash size distributions.

Fig. 10. Theoretical and observed dependence of the extinction-to-mass ratio of fly ash aerosols on particle size and wavelength of the light source.

and white smoke plumes. A combustion smoke generator designed for training of smoke inspectors was used to produce spherical particles. The chemical composition of the fuel determined whether black or white smoke was emitted. Plume opacity (1.0 − transmission) measurements were derived from the lidar signature by comparing clear-air returns from the near and far side of the plume return.[3] The opacity measurements are not strongly a function of plume particle composition. The plume returns, normalized to the near-side clear-air returns, depend strongly on plume particle composition. Therefore, as shown in Fig. 8, the ratio of plume backscatter to plume attenuation evaluated from lidar backscatter signatures identifies white smoke from black smoke. This method of cloud identification is based on absorption of light by the scattering particles. Particle backscatter is strongly affected by particle absorption, whereas particle extinction is only weakly affected by particle absorption.

Figure 9 illustrates another method of cloud identification. The receiver of the 0.7-μm wavelength Mark IX lidar system is easily polarized by placing a polarization filter over the receiver aperture. Because the emitted laser energy is linearly polarized, the depolarization of cloud backscatter can be evaluated by rotating the polarization filter to observe the cross- and parallel-polarization components. Polarization of the incident light is maintained for scattering from spherical particles but is destroyed for scattering from irregularly shaped particles. Therefore, as shown in Fig. 9, the difference between cross and parallel components of backscatter is greater for water clouds (factor of 6.8) than for dust clouds (factor of 4). These data indicate that lidar can be used to distinguish between water and dust clouds from remote distances. Other investigators have demonstrated the use of polarized lidar systems for cloud studies.[4,5]

V. Lidar Evaluation of Cloud Physical Density

Relationships between the optical and physical parameters of clouds typically depend on particle size, shape, and composition distributions. Therefore, inferences of cloud physical density from cloud backscatter or attenuation measurements are subject to uncertainties introduced by unknown properties of the scattering particles. Recent research efforts have been directed to the development of optical techniques for aerosol density analysis that minimize uncertainties introduced by particle characteristics. For example, Fig. 10 presents measured and computed values of the extinction-to-mass concentration ratio as a function of wavelength for fractions of fly ash aerosols of different sizes.[6] Computed values agree well with measured values for visible and 3.39-μm (He–Ne laser) wavelengths. These data indicate that an optimum wavelength exists for relating aerosol extinction measurements to aerosol mass concentration independent of particle size uncertainties.

Figure 11 presents extinction-to-volume concentration measurements as a function of mean particle size for both visible and 3.39-μm wavelengths. (Sauter diameter is defined by the ratio of the third and second moment of the particle size distribution.) Data were collected for four sizes of fly ash fractions, three sizes of silica fractions, and an iron oxide fraction of one size.[6] Although these particles vary greatly in size, shape, and composition, the data presented in Fig. 11 indicate that a lidar extinction measurement at 3.39 μm provides a good estimate of aerosol volume concentration for all aerosol types used in this experiment.

To investigate the use of lidar for quantitatively

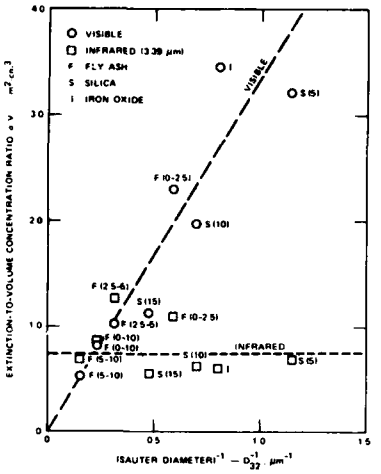

Fig. 11. Extinction-to-volume concentration ratios as a function of particle size for visible and infrared (3.39-μm) wavelengths.

evaluating the emission rate of fugitive particulate sources, an experiment was conducted with a controllable particle emission source.[7] The lidar made cross-plume observations similar to those shown in Fig. 1 at ~500 m downwind of the smoke source. In addition to the lidar observations, wind speed and direction were recorded at the lidar site. Cross-plume backscatter values were integrated and adjusted by wind speed and direction to provide an estimate of smoke emission rate. The smoke generator was used at three emission rates, and for each rate ~10–20 plume cross sections were recorded. Figure 12 shows that the resulting time-averaged cross-plume backscatter values were linearly related to the source emission rate. These results indicate the potential of lidar for monitoring smoke plume particle concentrations.

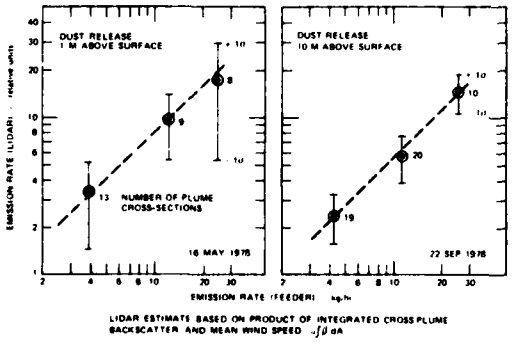

Fig. 12. Particulate emission rate evaluated from lidar plotted as a function of emission rate evaluated from particle feeder.

VI. Conclusions

Lidar provides the means to evaluate quantitatively the spatial and temporal variability of smoke and dust clouds. However, attenuation, multiple scattering, and unknown particle characteristics can introduce uncertainties in the interpretation of the lidar backscatter signature. For dense smoke clouds, longer wavelength systems are better suited because of lesser attenuation and multiple scattering.

The capability of lidar to make remote evaluations of cloud type, optical density, and physical density has been demonstrated. However, additional information or assumptions on the characteristics of the scattering particles generally are needed, and cloud density evaluations, therefore, are subject to uncertainties regarding particle characteristics.

The data examples presented in this paper were collected with ground-based mobile lidar systems, but aircraft-mounted systems offer substantial advantages in many applications. Recently, an airborne lidar system (ALPHA-1: Airborne Lidar Plume and Haze Analyzer) was used to track aerosol plumes to long downwind distances from their sources and to observe the distribution of aerosol layers over large regional areas.[8] An example of plume tracking is presented in Fig. 13 for a plume that was subvisible only a few kilometers downwind of the source. The ALPHA-1 system operates simultaneously at two wavelengths (1.06 and

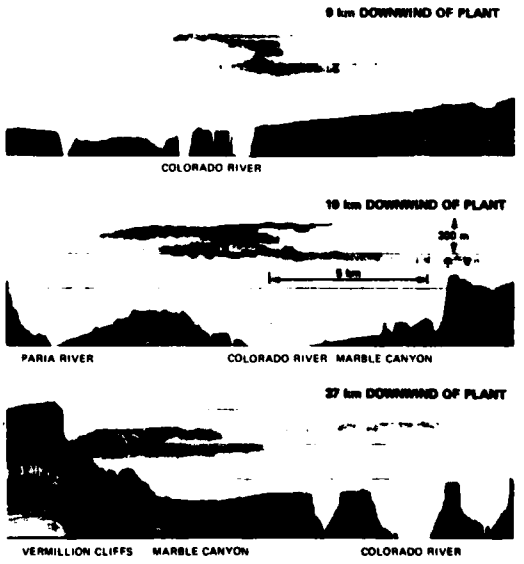

Fig. 13. Airborne lidar observations of the cross-plume structure of a subvisible power plant plume at different downwind distances from the plant (1.06-μm lidar wavelength).

0.53 μm) to provide additional information needed to estimate aerosol optical and physical parameters. Other multiple wavelength systems are currently under consideration for extending the lidar technique so that it can be used more widely in the evaluation of aerosol clouds.

The Smoke Week II lidar experiment was funded by the U.S. Army Research Office, Geosciences Division, with additional support provided by the U.S. Army Atmospheric Sciences Laboratory. Other data were obtained from projects with the U.S. Environmental Protection Agency, U.S. Air Force, and the Electric Power Research Institute.

References

1. R. T. H. Collis and P. B. Russell in *Laser Monitoring of the Atmosphere*, E. D. Hinkley, Ed. (Springer, New York, 1976), p. 71.
2. E. E. Uthe, Proc. Soc. Photo-Opt. Instrum. Eng. **142**, 67 (1978).
3. C. S. Cook, G. W. Bethke, and W. D. Conner, Appl. Opt. **11**, 1742 (1972).
4. S. R. Pal and A. I. Carswell, Appl. Opt. **12**, 1530 (1973).
5. K. Sassen, J. Appl. Meteorol. **17**, 73 (1978).
6. E. E. Uthe, APCA J. **30**, 382 (1980).
7. E. E. Uthe, C. E. Lapple, C. L. Witham, and R. L. Mancuso, Third Symposium on Fugitive Emissions Measurement and Control, EPA Report 600/7-79-182 (1979), pp. 431–442.
8. E. E. Uthe, N. B. Nielsen, and W. Jimison, Bull. Am. Meteorol. Soc. **61**, 1035 (1980).

Appendix B

PARTICLE SIZE EVALUATIONS USING MULTIWAVELENGTH EXTINCTION MEASUREMENTS*

*Applied Optics, Vol. 21, pp. 454-459 (1982).

Reprinted from APPLIED OPTICS, Vol. 21, page 454, February 1, 1982

Particle size evaluations using multiwavelength extinction measurements

Edward E. Uthe

As the first phase of a program to develop a lidar method for remote evaluation of mean particle size of stationary source emissions, a data base was experimentally collected consisting of multiple-wavelength extinction coefficients and mean particle sizes of generated aerosols. Extinction data were collected using multiwavelength (14) transmissometers and a 10-m long aerosol tunnel facility. Generated aerosols consisted of five size fractions of fly ash, three size fractions of silica, and single-size fractions of six other types of particulate material. Particle size evaluations were made by multistage impactor and by air permeability (Fisher) analysis of packed powder. The data base indicates that mean particle size smaller than 1-μm diam could be estimated usefully from aerosol extinction measurements using a single-laser lidar system operating at 1.06- and 0.53-μm wavelengths. For larger mean particle sizes the extinction ratio is near unity, and longer wavelength systems are required. The data indicate that a two-laser lidar operating at 10.6 and 0.53 μm could provide estimates of mean particle size to diameters of at least 6 μm.

I. Introduction

Characteristics of particulate emissions from stationary sources are generally determined by in-stack sampling methods that provide information at only a single location within the stack and therefore require traversal of the stack to obtain a representative sample. Such methods are difficult to apply without affecting particle concentrations or size distributions and have no potential for remote measurement applications for enforcement of particulate emission standards.

White-light cross-plume transmissometers are widely used to monitor stack emissions. Instrumented in-stack measurements can be used for abiding by plume opacity or visual standards. In addition, plume opacity can be extended to remote off-site observations using lidar techniques.[1-3]

It may be possible to apply transmissometer and lidar opacity techniques for providing additional characterization of stationary source emissions. For example, recent experimental results indicate that an IR transmissometer can be used to monitor particulate mass emissions.[4] Other studies have indicated that multiple-wavelength systems can provide information on particle size distributions.[5,6]

The experimental study reported in this paper employed a 14-wavelength transmissometer to demonstrate that multiwavelength extinction measurements can be interpreted in terms of mean particle size of observed aerosols. The study represents the first phase of a program designed to apply lidar techniques for remote evaluation of the mean particle size of stationary source emissions.

II. Experimental Facilities and Procedures

A. Transmissometers

Multiple-wavelength transmission measurements were made using instrumentation readily available from other projects. Wavelengths and additional transmissometer information are provided in Table I. Included were a multiple-wavelength (0.39–1.64-μm) sunphotometer, an IR photometer (3.9 μm), and IR He–Ne (3.39-μm) and carbon dioxide (10.6-μm) continuous wave lasers. The photometers employed wideband photodiode detectors operating in the photovoltaic mode with wavelength response determined by narrowband (~10-nm) filters. A zirconium arc lamp (100 W) was used as a broadband light source. A liquid-nitrogen-cooled HgCdTe detector was employed in the He–Ne and CO_2 laser receiver which alternately observed each wavelength by a chopper arrangement. A photopic (eye-response) transmissometer was available from a previous study. Field of view of each transmissometer receiver was minimized (typically 2°) to reduce effects of forward scattering on transmission measurements.

The author is with SRI International, Atmospheric Science Center, Menlo Park, California 94025.
Received 5 September 1981.
0003-6935/82/030459-06$01.00/0.

Table I. Transmissometer Specifications

Wavelength (nm)	Bandwidth (nm)	Source	Detector
390	20	Zirconium arc lamp	Silicon photodiode
450	19.6	Zirconium arc lamp	Silicon photodiode
514	18.6	Zirconium arc lamp	Silicon photodiode
613	7.8	Zirconium arc lamp	Silicon photodiode
670	11.3	Zirconium arc lamp	Silicon photodiode
870	12.6	Zirconium arc lamp	Silicon photodiode
930	14.	Zirconium arc lamp	Silicon photodiode
1045	18.8	Zirconium arc lamp	Silicon photodiode
1240	10.7	Zirconium arc lamp	Germanium photodiode
1640	15.	Zirconium arc lamp	Germanium photodiode
3390	<0.01	He–Ne laser	HgCdTe
3900	156.	Zirconium arc lamp	PbSe photodiode
10600	<0.01	CO_2 laser	HgCdTe
Photopic	Eye response	Tungsten lamp	Silicon photodiode

B. Calibration and Data Recording

An Esterline Angus model PD-2064 data logger was used to sample transmissometer output voltages and write digital values on magnetic tape. Voltage levels at 0 and 100% transmission were determined before each data collection run from data for clear air paths and complete blockage of the source energy. Transmissometer response was evaluated with neutral density filters, and all channels were found to be linear within ±0.5 dB over the 0–100% range. Therefore, the instruments were assumed linear in all subsequent data reduction and analysis.

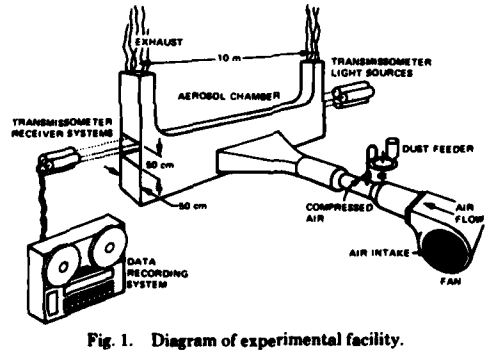

Fig. 1. Diagram of experimental facility.

C. Aerosol Tunnel

The transmissometers were mounted across a 10-m long aerosol tunnel that was designed with open ends to facilitate transmissometer and lidar experiments. Figure 1 presents a diagram of the experimental facility. Particulate material was metered out by a grooved disk feeder with a powder feed rate controlled by disk rotation speed. The material was dispersed via a nozzle operated at sonic velocity into a 164-m^3 (5800-ft^3)/min airflow generated by a centrifugal blower. Dust-laden air was gradually decelerated into an expanding ductwork and allowed to enter a plenum chamber beneath the aerosol sighting tunnel. Two nozzles located at the chamber ends generated aerosol-laden air curtains to carry away any outside air blown into the tunnel and thus establish a fixed boundary for the dust-laden air in the sighting tunnel. A perforated plate in the center of the chamber provided for uniform distribution of air into the tunnel without significant particle loss. The air moved from the center section toward the aerosol

Table II. Size Properties of Test Aerosols

Type	Cascade Impactor Mass Median Diameter (μm)	Standard Geometric Deviation[a]	Sauter Diameter (μm)	
			Impactor	Fisher[b]
0–10-μm fly ash	3.7	2.1	2.8	4.1
5–10-μm fly ash	5.1	2.0	3.9	5.8
2.5–5-μm fly ash	2.3	1.5	2.1	3.2
0–2.5-μm fly ash	1.6	2.1	1.1	1.6
Superfine fly ash	0.85	1.7	0.75	0.79
5-μm silica	0.7–2.0	2.4–5.0	0.4–0.8	0.84
10-μm silica	1.3	3.3	0.6	1.45
15-μm silica	2.3–7.0	2.9–5.0	1.0–1.9	2.1
Iron oxide	0.9–2.0	5–12	0.08–0.2	0.73
Ammonium chloride	0.4	3.8	0.2	—
Zinc chloride	0.5	1.5	0.4	—
Titanium oxide	0.3	2.0	0.2	—
Aluminum	2.0	1.3.	1.9	—
Rosin	~12	~60	0.003	—

[a] Standard geometric deviation was determined from the best-fit log-normal size distribution.
[b] From Fisher subsieve size analysis of bulk powders before aerosolization.

curtains and out the exhaust stacks. The tunnel previously has been used on several transmissometer and lidar development and evaluation projects[4,7,8]; further details of its design and operation are available.[9]

D. Test Aerosols

Table II lists types of aerosols that were generated for observation by the multiple-wavelength transmissometers. The ground silica, fly ash, iron oxide, aluminum, and titanium dioxide were all dispersed from the disk feeder as dry powders. Ammonium chloride aerosol was generated by mixing the vapors from solutions of ammonium hydroxide and hydrochloric acid. Zinc chloride aerosol was obtained from commercially available smoke candles. Rosin smoke was made by heating rosin until it fumed and sweeping the vapor into the chamber with a cold airstream, resulting in condensation of rosin particles.

E. Particle Size Evaluations

The dust-laden air was sampled for particle size in the ductwork just before the air entered the tunnel. Linear sampling velocity was matched to airflow in the duct to approximate isokinetic sampling conditions. To condition the sampling system with equilibrium temperature and humidity, a continuous airstream was drawn from the ductwork through the sampler for long periods of time before particle size sampling was initiated. The conditioning air was filtered to remove particulate material and routed to a multistage piezoelectric cascade impactor manufactured by California Measurements, Inc. Particulate samples were taken by running unfiltered air from the ductwork directly through the impactor. Aerosol concentration data were obtained from open-faced filter samples taken through the same sampling port that was used to collect the impactor samples.

The impactor data provide information on the mass median diameter of the particle size distribution and the effective standard geometric deviation (width of a log-normal particle size distribution). Sauter diameters (volume-to-surface mean diameters)[10] can be obtained from these results assuming a log-normal particle size distribution. Sauter diameters also were determined directly by applying air permeability (Fisher subsieve size) analysis to packed powder. Particle size results averaged over several measurements are presented in Table II.

Table III. Examples of Wavelength Extinction Measurements*

Aerosol Type	Extinction Coefficient (km^{-1}) at Indicated Wavelength (μm)													
	Photopic	0.390	0.450	0.514	0.613	0.670	0.870	0.930	1.045	1.24	1.63	3.39	3.90	10.6
0–10 μm fly ash	83.3	78.2	78.2	78.7	79.6	80.1	83.1	84.7	86.7	90.8	90.6	74.1	71.3	53.2
5–10 μm fly ash	63.5	54.9	56.7	58.3	59.7	60.1	61.6	61.8	62.4	63.5	63.6	67.1	70.3	54.7
2.5–5 μm fly ash	86.6	81.0	81.9	82.7	83.5	83.7	86.8	87.8	89.4	92.8	100.2	94.9	85.6	47.4
0–2.5 μm fly ash	63.5	60.8	60.3	60.5	61.5	62.8	68.6	71.0	75.0	79.7	76.5	29.8	23.9	13.6
Superfine fly ash	98.9	98.1	98.8	98.8	97.8	96.3	89.7	87.5	82.7	72.1	56.7	14.4	13.9	10.1
5 μm silica	90.5	95.7	94.5	92.5	88.9	86.4	78.6	76.1	71.5	63.4	52.3	14.7	11.1	8.3
10 μm silica	71.0	77.7	74.7	71.1	66.8	64.8	58.8	57.2	54.4	50.9	43.0	22.4	20.0	14.8
15 μm silica	95.5	92.8	92.8	92.2	91.0	90.6	86.8	85.7	83.4	81.4	72.3	35.5	39.6	34.1
Iron oxide	117.7	102.7	107.7	113.6	117.7	116.1	102.3	97.4	88.6	74.1	55.2	19.3	17.0	8.2
Ammonium chloride	97.4	134.6	134.9	113.3	90.1	79.0	51.3	45.6	37.2	26.0	16.2	9.5	3.1	0.7
Zinc chloride	76.8	75.2	77.3	77.7	74.8	71.5	58.1	54.1	47.0	35.6	22.0	6.4	3.5	2.2
Titanium dioxide	340.6	260.1	285.1	320.6	367.0	349.3	304.5	282.3	262.3	175.4	101.3	11.10	6.2	4.1
Aluminum	66.4	58.0	59.7	61.4	62.4	62.6	64.0	63.9	63.5	65.6	62.6	58.1	61.3	56.6
Resin	11.0	27.2	19.7	14.3	9.9	8.3	4.9	4.3	3.5	2.3	1.6	—	0.1	—

* Arbitrary mass concentrations used for each aerosol measurement.

III. Experimental Results

A. Wavelength Dependence of Extinction

Magnetic tape records of digitized voltages produced from the transmissometer array were reduced in terms of aerosol extinction coefficients σ assuming linear response of the transmissometers and from voltage levels corresponding to 0 and 100% transmission T and $\sigma = -1/L \ln T$, where the path length $L = 10$ m. No correction was applied for multiple-scattering effects. Neutral density filters of known transmission of ~50%

were periodically used to check transmissometer response. Typically, data collection runs were conducted with three arbitrary levels of aerosol concentration to avoid evaluating extinction coefficients from either very high or low transmission values.

Typical wavelength-dependent extinction coefficients are given in Table III for each of the test aerosols listed in Table II. Figure 2 presents a plot of extinction coefficients as a function of wavelength; data are derived from several experimental runs using different types of particulate material. Coefficients derived from the photopic response transmissometer are plotted at a wavelength of 0.55 μm, although the plotted data indicate a slightly longer effective wavelength of 0.58 μm. For these data iron oxide particulates had the largest diameters (Fisher analysis of 0.73-μm diam) and exhibited less wavelength dependency than the other particulates. Zinc chloride, ammonium chloride, and rosin had progressively smaller particle sizes accompanied by progressively stronger dependence of the extinction coefficient on wavelength.

Figure 3 presents extinction-to-mass (σ/M) concentration ratios as a function of wavelength derived from transmission data for fly ash aerosols. The mass concentration was derived from the photopic transmissometer readings and previously determined extinction-to-mass concentration ratios evaluated from time-averaged data collected with this instrument.[9] The data presented in Fig. 3 show that the extinction-to-mass ratio is strongly dependent on particle size at short wavelengths but is nearly independent of particle size at long IR wavelengths. Previous data derived from the photopic and 3.39-μm transmissometers provided similar results, while a theoretical analysis indicated that σ/M would significantly increase with particle size at the 10.6-μm wavelength.[4] A wavelength region with σ/M independent of particle characteristics is important for development of a method to monitor particulate mass concentrations. The results presented in Figs. 2 and 3 indicate that for particles smaller than 1 μm, the greatest wavelength dependence of extinction is at longer wavelengths, and for particles 1–3 μm in size, the greatest wavelength dependence is in the 1–4-μm wavelength range.

B. Evaluation of Particle Size from Extinction Data

Several authors have addressed the problem of estimating particle size distribution $n(a)$ from multi-wavelength extinction or scattering observations $\sigma(\lambda)$.[11-13] Basically, this involves solving a linear matrix equation of the form

$$\sigma(\lambda_i) = \sum_j K(\lambda_i, a_j) n(a_j) + E_i,$$

where the matrix K is derived from theoretical considerations, and the E_i are measurement errors. Formal solution techniques are not required to demonstrate that mean particle size $\bar{a}$ can be estimated from $\sigma(\lambda)$, although calculating $\bar{a}$ from $n(a_j)$ would optimize usage of the information content provided by the measurements $\sigma(\lambda_i)$.

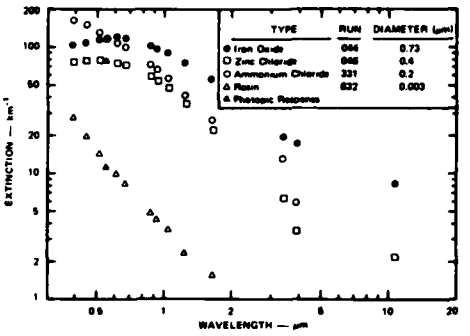

Fig. 2. Extinction as a function of wavelength for various smokes of different particle sizes (particle Sauter diameter determined from impactor measurements).

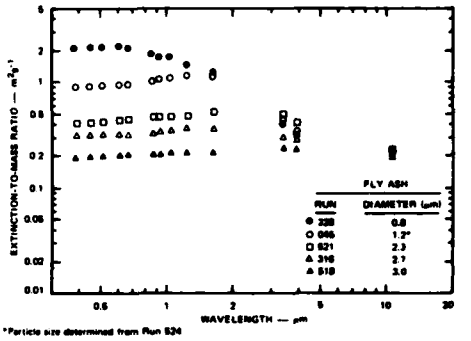

Fig. 3. Extinction-to-mass concentration as a function of wavelength for various particle size fractions of fly ash (particle Sauter diameter determined from impactor measurements).

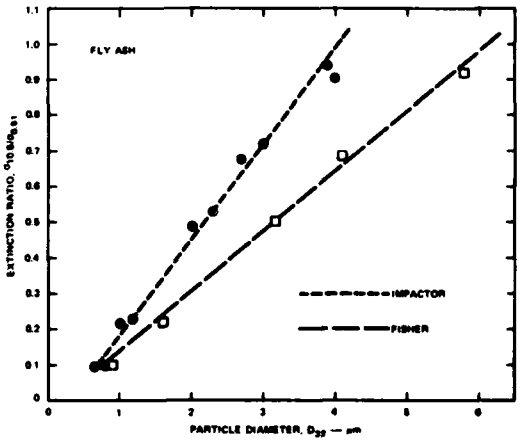

Fig. 4. Ratio of extinction at 10.6- and 0.51-μm wavelengths as a function of mean (Sauter) diameter for fly ash aerosols.

For this study we have chosen to relate the ratio of extinction values observed at laser or near-laser wavelengths to independently evaluated particle size data. Figure 4 presents a plot of the ratio of extinction coefficients for fly ash aerosols observed at 10.6- and 0.51-μm wavelengths as a function of Sauter mean diameter. These data show that the extinction ratio is linearly related to the Sauter mean diameter evaluated from either the impactor or Fisher permeability analysis. Particle diameters evaluated by the two methods used in this study are in approximate agreement for particles smaller than 1 μm but disagree for larger particles with the difference directly proportional to particle size. This disagreement in particle size measurement between the two methods probably reflects an error in estimating the log-normal distribution curve and subsequently calculating the standard geometric deviation. The Sauter mean diameter calculated from the impactor measurement is dependent on the standard geometric deviation and the mass median diameter. The disagreement may also reflect the possibility that large particle bounce in the impactor indicated a lower than actual mass median diameter. These data indicate that CO_2 and neodymium harmonic laser wavelengths could be used for remote evaluation of mean particle size of fly ash emissions from stationary sources.

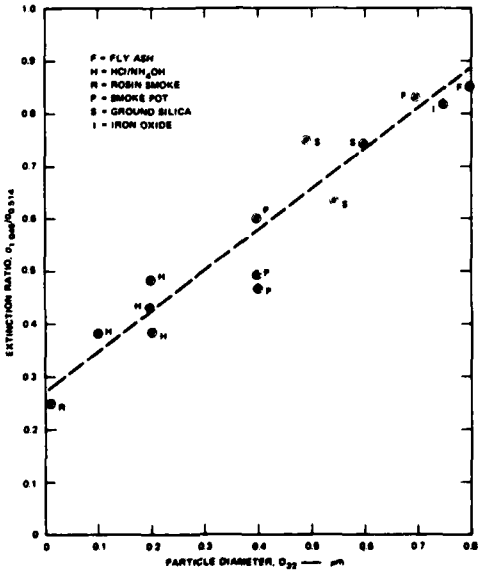

Fig. 5. Ratio of extinction at 1.045- and 0.514-μm wavelengths as a function of mean (Sauter) diameter (impactor measurements) for submicron particles of different compositions.

Figure 5 presents a plot of the ratio of extinction coefficients at 1.045- and 0.514-μm wavelengths as a function of Sauter mean diameter (impactor) derived from observations of generated aerosols with particle sizes <1 μm. These data indicate that this extinction ratio can be used as an indicator of particle size. The greater data scatter about the regression line than for the fly ash results shown in Fig. 4 probably results from particle composition and shape effects. The data presented in Fig. 5 indicate that a single laser system, Nd:YAG (1.06 μm) and its first harmonic (0.53 μm), would be useful to evaluate particles of sizes <1 μm.

The extinction ratio $\sigma_{1.045}/\sigma_{0.514}$ tends to converge to a value of 1.2 for particle sizes >1 μm (see Table III fly ash values) and therefore is not a good indicator of particle size for larger particles. The results of this study show that extinction ratios of less than unity are useful for estimating mean particle size. Extinction ratios near unity indicate larger particles and require longer wavelength extinction measurements for particle size analysis.

IV. Conclusions

An experimental study has been conducted to collect a data base consisting of multiple-wavelength extinction coefficients and mean particle diameters of generated aerosols representative of stationary source emissions. The data base indicates that the ratio of extinction coefficients can be used as a measure of mean particle size, providing the ratio of long wavelength to short wavelength extinction is less than unity. When the ratio is near unity, larger particles are present and still longer wavelength observations are needed.

The results of this study indicate that a lidar system using a single laser generating energy at 1.06- and 0.53-μm wavelengths can provide estimates of mean particle size for mean particle diameters smaller than 1.0 μm. Required lidar extinction measurements of stationary source emissions can be made by observation of clear-air backscattering on the far side of the plume particulate scattering. Therefore the results of this study indicate the feasibility of using a single-laser lidar system to make remote measurements of mean particle size of stationary source emissions having <1-μm mean particle diam. For emissions with mean particle diameters from 1 to 6 μm a two-laser system could be used for remote measurement of mean particle size.

This study was funded by the U.S. Environmental Protection Agency under contract 68-02-3267. William D. Conner, the contract technical monitor, provided helpful discussion on the experimental approach. Clyde L. Witham and Robert W. Gates were responsible for aerosol generation and characterization. William D. Dyer and Jan van der Lann implemented the transmissometer instrumentation; William D. Dyer also conducted the measurement program.

References

1. W. E. Evans, "Development of Lidar Stack Effluent Opacity Measuring System," NTIS PB 233-135/AS (U.S. Govt. Printing Office, Springfield, Va., 1967).
2. C. S. Cook, G. W. Bethke, and W. D. Conner, Appl. Opt. **11**, 1742 (1972).
3. W. D. Conner and N. White, Comparative Study of Plume Opacity Measurement Methods, Environmental Protection Agency report EPA-600/2-80-001 (1980).
4. E. E. Uthe, Air Pollut. Control Assoc. J. **30**, 382 (1980).
5. K. L. Cashdollar, C. K. Lee, and J. M. Singer, Appl. Opt. **18**, 1763 (1979).
6. F. C. Ariessohn, S. A. Self, and R. H. Eustis, Appl. Opt. **19**, 3775 (1980).
7. C. E. Lapple and E. E. Uthe, Remote Sensing of Particulate Stack Emissions, AIChE Symp. Ser. **72**, 181 (1976).
8. E. E. Uthe and W. E. Evans, "Lidar Calibration and Performance Evaluation," Environmental Protection Agency Final Report contract 68-01-4137 (Task 4) (SRI International, Menlo Park, Calif., 1979).
9. E. E. Uthe and C. E. Lapple, "Study of Laser Backscatter by Particulates in Stack Emissions," Environmental Protection Agency Final Report contract CPA 70-173, PB 212530 (1972).
10. C. E. Lapple, "Particle Size Analysis and Analyzers," Chem. Eng., **75**, No. 11, 149 (20 May 1968).
11. S. Twomey and H. B. Howell, Appl. Opt. **6**, 2125 (1967).
12. M. D. King, D. M. Byrne, B. M. Herman, and J. A. Reagan, J. Atmos. Sci. **35**, 2153 (1978).
13. G. Yamamoto and M. Tanaka, Appl. Opt. **8**, 447 (1969).

Appendix C

AIRBORNE LIDAR MEASUREMENTS OF SMOKE PLUME DISTRIBUTION, VERTICAL TRANSMISSION, AND PARTICLE SIZE*

*Applied Optics, Vol. 21, pp. 460-463 (1982).

Reprinted from APPLIED OPTICS, Vol. 21, page 460, February 1, 1982

Airborne lidar measurements of smoke plume distribution, vertical transmission, and particle size

Edward E. Uthe, Bruce M. Morley, and Norman B. Nielsen

Observations were made of a dense smoke plume downwind from a forest fire using the ALPHA-1 two-wavelength downward-looking airborne lidar system. Facsimile displays derived from lidar signatures depict plume dimensions, boundary layer height, and underlying terrain elevation. Surface returns are interpreted in terms of vertical transmission as function of cross-plume distance. Results show significantly greater plume attenuation at 0.53-μm wavelength than at 1.06-μm, indicating ~0.1-μm mean particle diameters or the presence of gaseous constituents that absorb the visible radiation. These results demonstrate the potential of multiple-wavelength airborne lidar for quantitative analysis of atmospheric particulate and gaseous constituents.

I. ALPHA-1 Airborne Lidar

An airborne lidar system has been designed, constructed, and applied to environmental studies for the Electric Power Research Institute. The ALPHA-1 (Airborne Lidar Plume and Haze Analyzer) is a downward-looking system flown aboard the SRI Queen Air, a twin-engine research aircraft with specialized navigational instrumentation and facilities for lidar applications. External and internal views of the ALPHA-1 aircraft are shown in Fig. 1. The lidar simultaneously transmits laser pulses at two wavelengths and receives range-resolved backscattered energy from the atmosphere and reflected energy from the earth's surface. The near IR wavelength (1.06 μm) is very sensitive to detection of low density (subvisible) particulate pollution because of the larger ratio of aerosol-to-molecular scattering at longer wavelengths. The shorter wavelength (0.53 μm) is used for deriving visibility related information and for applying two-wavelength analysis of backscatter signatures in terms of other aerosol parameters (e.g., extinction and concentration).

The ALPHA-1 data system uses dual microprocessors for data recording at high collection rates and real-time processing for height/distance pictorial (facsimile) display of atmospheric and terrain features. The lidar can be operated at a pulse rate of 10/sec, backscatter signatures at both wavelengths resulting from each pulse can be digitized to provide 2048 values with range resolution of 1.5 m. The fine vertical and horizontal resolution data are plotted in pictorial form and are available in real time [Fig. 1(b)] for directing the data collection. The signatures are also recorded on nine-track magnetic tape for later analysis of atmospheric behavior and aerosol physical and optical properties. System details and data examples have been presented elsewhere.[1,2]

II. Plume and Ground Observations

During a flight test of the ALPHA-1 observations were made downwind of a forest fire located near the California coast. Visually, the fire appeared to be contained within a small area; the resulting smoke plume towered over the source but was transported downwind at lower altitudes.

Three cross-plume flights were made with the ALPHA-1 system. The initial pass was made ~2 km downwind from the source with the lidar receiver systems operating at full gain. This resulted in observation of low-density background aerosol distributions; however, the receiver electronics were saturated by surface returns which typically exceed the background aerosol returns by 4 orders of magnitude. The second pass across the plume was made at about the same downwind distance but with reduced receiver gain so that the variability of surface returns could be observed and recorded. The third pass was made with less sensitive lidar receivers but was flown over the densest part of the plume—~500 m from the source.

Figure 2 is a facsimile plot of the IR signatures (logarithmic values) collected during the first ALPHA-1

The authors are with SRI International, Atmospheric Science Center, Menlo Park, California 94025.
Received 25 September 1981.
0003-6935/82/030460-04$01.00/0.

(a) EXTERIOR VIEW

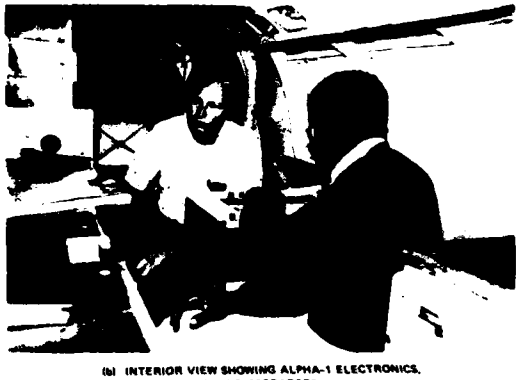

(b) INTERIOR VIEW SHOWING ALPHA-1 ELECTRONICS, DISPLAY UNIT, AND OPERATORS

Fig. 1. ALPHA-1 aircraft.

flight across the smoke plume. The plume base coincides with the top of a haze layer ~600 m above the surface. Haze layer tops normally indicate temperature inversions that restrict vertical transport of atmospheric constitutents.[3] Particulate material from the fire penetrated the inversion and was transported downwind above the inversion level. The most buoyant part of the plume extended to ~1900 m above the surface.

III. Transmission Analysis and Interpretation

Figure 3 shows plume cross sections derived from IR and visible backscatter sigratures recorded during the second pass of ALPHA-1 across the plume. Greater plume attenuation of the visible energy than that experienced by the IR energy is evident by the absence of plume visible backscatter following penetration by the laser pulse of the denser plume elemer s. Plume transmissions in the vertical were evaulated by normalizing to 100% the surface returns in the absence of plume backscatter and assuming constant surface reflectivity and laser transmitted peak power for each laser firing made along the cross-plume path. Lidar response information required for quantitative analysis of backscatter signatures was derived using standard

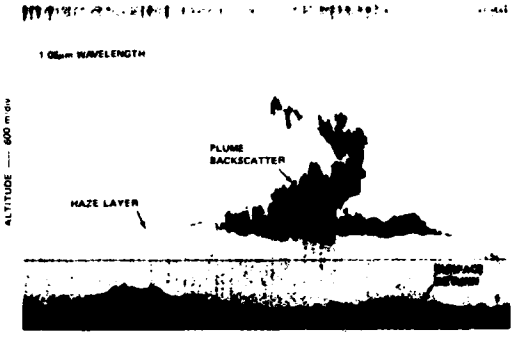

Fig. 2. Cross-plume structure derived from ALPHA-1 plume backscatter at 1.06-μm wavelength (aircraft pass 1).

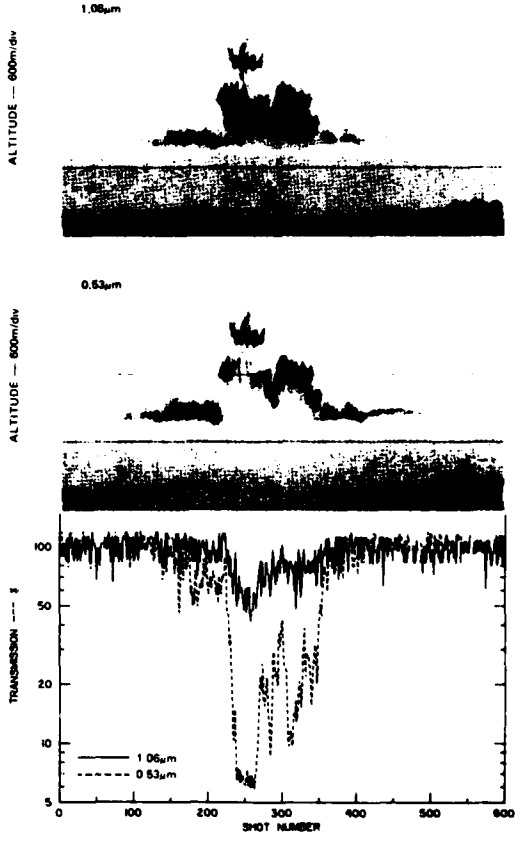

Fig. 3. Cross-plume structure derived from ALPHA-1 plume backscatter and vertical transmissions derived from surface returns at 1.06- and 0.53-μm wavelengths (aircraft pass 2).

calibration techniques with natural density filters of known attenuation. Vertical transmission for one-way passage of the laser energy through the smoke plume are plotted in Fig. 3. The results show minimum plume transmissions of ~50% at 1.06 μm and ~6% at 0.53 μm. The strong wavelength dependence of attenuation suggests submicron particle sizes, although strong absorption in the visible and weak absorption in the IR by plume constituents could also explain the observations.

Figure 4 shows IR and visible wavelength facsimile records and transmission analysis derived from data collected during the third pass across the plume. This pass was made nearer to the source (~500 m) over the densest part of the plume, as determined visually. Greater plume density, increased vertical dimensions, and reduced horizontal dimensions nearer to the source

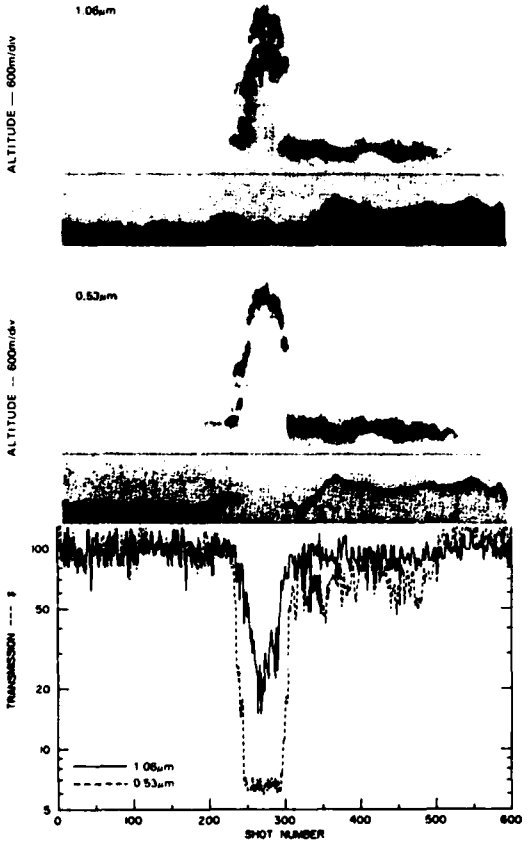

Fig. 4. Cross-plume structure derived from ALPHA-1 plume backscatter and vertical transmissions derived from surface returns at 1.06- and 0.53-μm wavelengths (aircraft pass 3).

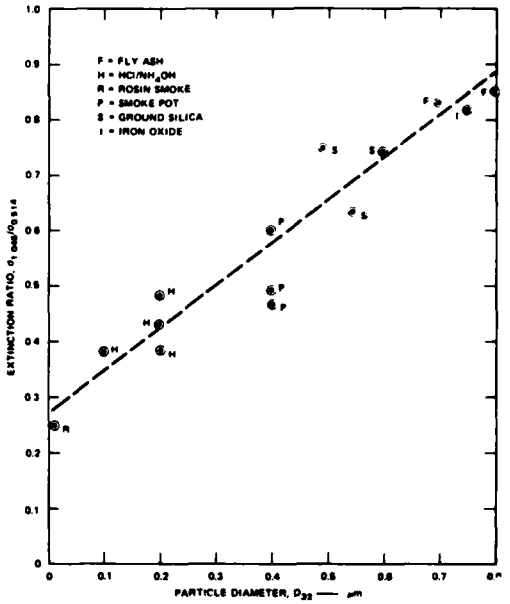

Fig. 5. Relationship of extinction ratio at 1.045- and 0.514-μm wavelengths and mean particle diameter derived from laboratory results.[4]

are clear in Fig. 4. Because the green wavelength surface returns were below the receiver noise level, minimum transmission were probably <5%. Minimum IR transmissions were ~15%. Lower visible transmissions could have been measured by removing the receiver gain reduction; however, the surface returns for clean air regions would have saturated the receiver system. A greater receiver dynamic range is needed for ground return experiments over dense aerosol plumes.

Analysis of the ALPHA-1 two-wavelength topographic returns shows that the smoke plume attenuated the green laser energy significantly more than the near IR laser energy. One possible explanation is that the scattering particles were sufficiently small in size to introduce the observed wavelength dependence. Figure 5 shows laboratory data relating the ratio of light extinction at 1.045 and 0.514 μm to particle diameter.[4] These are near the 1.06- and 0.53-μm wavelengths of the ALPHA-1 system and indicate that the observed differences in extinction may be explained by small particle sizes. The ratio of optical depths ($u = -\ln T$) at 1.06- and 0.53-μm wavelengths derived from the plume transmission T data in Fig. 3 are betwen 0.2 and 0.3. Therefore, particle diameters smaller than 0.1 μm are indicated by the relationship of Fig. 5. Verification data were not collected on this experiment; however, previous in-plume sampling of combustion aerosols has found mean particle diameters in this size range. Mean particle sizes of combustion smokes have been measured as 0.002–0.3-μm diam,[5] the wide size range possibly

resulting from particle agglomeration near the source. MacArthur[6] found most particles from brush fires to have diameters near 0.1; this was later verified by Vines *et al.*[7] However, recent measurements by Stith *et al.*[8] indicate a 0.3-μm volume-to-surface area mean diam. downwind of burning forest slash. Cashdollar *et al.*[9] found mean particle sizes of 0.1 μm from wood fires. Therefore, the particle size derived from the ALPHA-1 measurements agrees well with previous data.

Another possible explanation of the greater plume attenuation at the visible than at the near IR wavelength is absorption by plume constituents. For example, NO_2 is a product of combustion and has greater absorption at 0.53 μm than at 1.06 μm. Therefore, the wavelength-dependent attenuation observed by ALPHA-1 could be (at least partially) a result of the presence of NO_2 or other constituents with similar optical properties. Differential absorption lidar (DIAL) systems have been developed that use closely spaced wavelengths located in strong and weak absorption spectra of gas species for remote measurement of gas concentrations.[10,11] The two-wavelength ALPHA-1 measurements may be similarly interpreted, although wide wavelength spacing is used.

IV. Conclusions

Previous studies have shown that the airborne lidar technique is perhaps the best method available for analysis of plume transport and diffusion downwind of particulate sources. The results presented in this paper show that plume transmissions for vertical paths can be evaluated from topographic lidar returns observed with airborne lidar systems. Moreover, multiple-wavelength transmissions can be interpreted in terms of information on plume gas and aerosol concentrations and on mean particle size. Further information on aerosol properties and particle concentration distributions can usually be derived from plume backscatter.[12] Coordinated airborne lidar and in-plume sampling is needed for validation of plume aerosol and chemical properties derived from multiple-wavelength lidar signature analysis.

The data presented in this paper were collected during a flight-test of the ALPHA-1 airborne lidar system for the Electric Power Research Institute. Data analysis was supported by SRI International.

References

1. E. E. Uthe, N. B. Nielsen, and W. L. Jimison, Bull. Am. Meterol. Soc. **61**, 1035 (1980).
2. E. E. Uthe, W. L. Jimison, and N. B. Nielsen, "Development of an Airborne Lidar for Characterizing Particle Distribution in the Atmosphere," Electric Power Research Institute Rep. EA-1538 (1980).
3. W. Viezee and J. Oblanas, J. Appl. Meterol. **8**, 369 (1969).
4. E. E. Uthe, "Particle size evaluation using multiwavelength extinction measurements," Appl. Opt., **21**, 000 (1982).
5. G. M. Byram and G. M. Jimison, U.S. Dept. of Agriculture Technical Bulletin (1948) p. 954.
6. D. A. MacArthur, Aust. For. **30**, 274 (1966).
7. R. G. Vines, L. Gibson, A. B. Hatch, N. K. King, D. A. MacArthur, and R. J. Taylor, Division of Applied Chemistry Technical Paper 1 (Commonwealth Scientific and Industrial Reseach Organization, Australia, 1971).
8. J. L. Stith, L. F. Radke, and P. V. Hobbs, Atmos. Environ. **15**, 73 (1981).
9. K. L. Cashdollar, C. K. Lee, and J. M. Singer, Appl. Opt. **18**, 1763 (1979).
10. R. T. H. Collis and P. B. Russell, in *Laser Monitoring of the Atmosphere*, E. D. Hinkley, Ed. (Springer, New York, 1976).
11. J. G. Hawley, L. D. Fletcher, G. F. Wallace, and H. Heron, "A Mobile Differential Absorption Lidar (DIAL) for Range Resolved Measurements of SO_2, O_3, and NO_2," in *Extended Abstracts Tenth International Laser Radar Conference* (American Meteorolical Society, Boston, 1980).
12. E. E. Uthe, Appl. Opt. **20**, 1503 (1981).


DATE
ILME